The Magnetotail Constellation Mission…

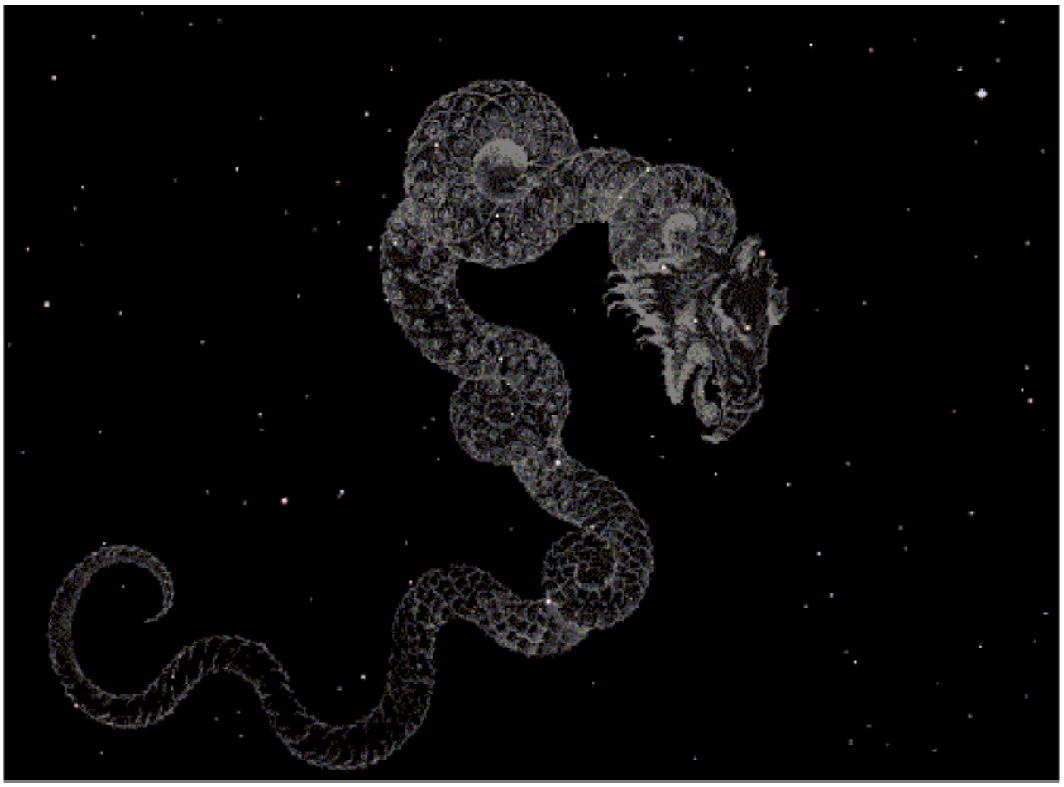

Dynamics, Reconnection, And Configuration Observatory (DRACO)

Resolving Complex Plasma Dynamics In Earth's Vast Magnetotail

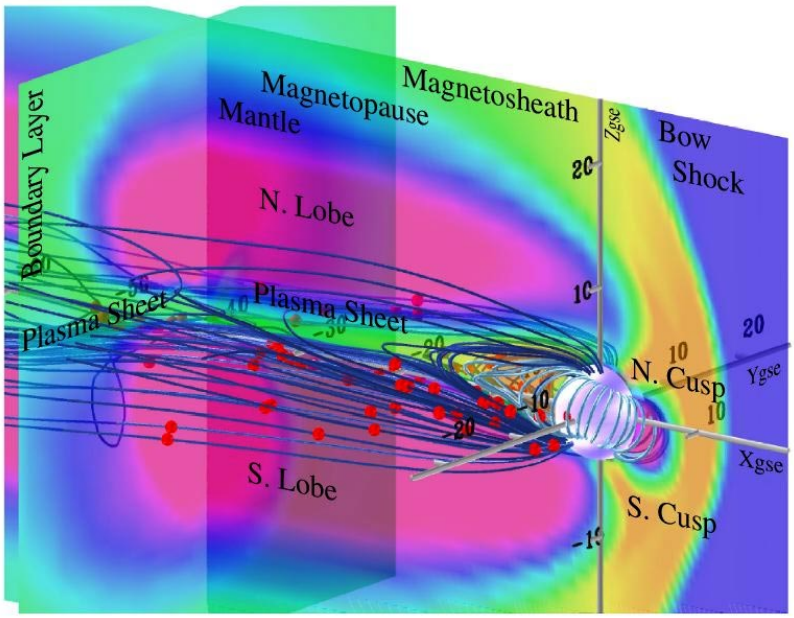

Report of the NASA Magnetospheric Constellation Science and Technology Definition Team

November, 1999

Table of Contents

Science and Technology Definition Team

Chairman
Harlan E. Spence
Dept. of Astronomy and Center for Space Physics
Boston University
Boston, MA

Project Study Scientist
Thomas E. Moore
Laboratory for Extraterrestrial Physics
NASA Goddard Space Flight Center
Greenbelt, MD

Project Formulation Manager
John P. Galloway
NASA Goddard Space Flight Center
Greenbelt, MD

Committee Members

Brian J. Anderson
Applied Physics Laboratory
Johns Hopkins University
Laurel, MD

Vassilis Angelopoulos
Space Sciences Laboratory
University of California, Berkeley
Berkeley, CA

Wolfgang Baumjohann
Max Planck Institute for
Extraterrestrial Physics
Garching, Germany

Joseph Borovsky
Space and Atmospheric Science
Los Alamos National Laboratory
Los Alamos, NM

Robert Carovillano
Department of Physics
Boston College
Chestnut Hill, MA

Paul D. Craven
Space Science Department
NASA Marshall Space Flight Center
Huntsville, AL

Joseph F. Fennell
Space Particles and Fields
The Aerospace Corporation
El Segundo, CA

Charles C. Goodrich
Department of Physics and Astronomy
University of Maryland
College Park, MD

Michael Hesse
Electrodynamics Branch
NASA Goddard Space Flight Center
Greenbelt, MD

Xinlin Li
Laboratory for Atmospheric and Space Physics
University of Colorado, Boulder
Boulder, CO

Kristina Lynch
Department of Physics
University of New Hampshire
Durham, NH

Peter Panetta
Systems, Technology, and Advanced Concepts
NASA Goddard Space Flight Center
Greenbelt, MD

Joachim Raeder
Institute for Geophysics and Planetary Physics
University of California, Los Angeles
Los Angeles, CA

Geoffrey Reeves
Space and Atmospheric Science
Los Alamos National Laboratory
Los Alamos, NM

David Sibeck
Applied Physics Laboratory
Johns Hopkins University
Laurel, MD

George Siscoe
Dept. of Astronomy and Center for Space Physics
Boston University
Boston, MA

Nikolai Tsyganenko
Raytheon
NASA Goddard Space Flight Center
Greenbelt, MD

David T. Young
Instrument and Space Research Division
Southwest Research Institute
San Antonio, TX

Solar Terrestrial Probes Program Scientist
Richard R. Vondrak
NASA Goddard Space Flight Center
Greenbelt, Maryland

Solar Terrestrial Probes, Geospace Probes Program Scientist
James A. Slavin
NASA Goddard Space Flight Center
Greenbelt, Maryland

Acknowledgments

The Magnetospheric Constellation Science and Technology Definition Team (MCSTDT) would especially like to thank the unwavering support, bold direction, and visionary leadership provided by the following NASA team members:

- Dana Brewer, Advanced Technology and Mission Studies, NASA Headquarters
- George Withbroe, Solar Terrestrial Probes Program Scientist; NASA Headquarters
- Lawrence Zanetti, Magnetospheric Constellation Program Scientist, NASA Headquarters

Without their dedicated and deliberate service to the space science community, the financial resources, administrative support, and agency impetus for this study and mission would clearly not have been possible. In addition, the MCSTDT gratefully thanks the previous pioneering efforts of Magnetospheric Constellation planning provided by NASA's Geospace Multiprobes Science and Technology Definition Team. We would also like to thank both the former and current NASA Office of Space Science Roadmap Teams, as well as the more informal community-based, but no less important, constellation development efforts within the space science community-at-large. Finally, we also would like to recognize all those scientists and engineers who, over the past 40 years of research and development, have provided the scientific basis, technological readiness, and insights needed to embark on this next millenial, mission.

"Looking to the future I believe that progress requires bunches of satellites, though these are as yet in no published program. One is continually conscious of this need for reasons which have a direct analogue on the ground…[S]ince satellites are being launched singly, the scientific returns are less than they could be." ***J. Dungey [1966]*** [(1)]

"Most of the important phenomena involve simultaneous variations in space and time. In some cases simultaneous measurements made at two well-chosen locations will provide unambiguous results. In other cases, it may be necessary to make simultaneous measurements at several hundred locations."
C. E. McIlwain [1967] [(2)]

….Yesterday's Future is <u>Now</u>!

(1) from "Inaugural Lecture as Professor of Physics at Imperial College", 1966; quote courtesy of W. J. Hughes.
(2) from "Comments and Speculations concerning the Radiation Belts", page 303 (Proceedings of the Joint IQSY/COSPAR Symposium, London, 1967, Part 1), MIT Press, 1967; quote courtesy of R. B. Sheldon.

Executive Summary

Magnetotail Constellation DRACO is the Solar Terrestrial Probe (STP) mission designed to resolve controversies concerning the complex dynamics of the magnetotail, open for 30 years for lack of suitable observations. Why is the magnetotail so structured and variable? How much of that structure and variation is imposed by the solar wind? Is the magnetotail inherently unstable? How and where are any instabilities triggered and propagated? In short, how does the magnetotail store, transport, and release matter and energy? To achieve observational closure with theory, we must distinguish spatial structures from temporal variations throughout the magnetotail. This requires a large number of small yet highly capable spacecraft, creating a station network capable of resolving 2 R_E scales at 10 sec time resolution, over a 15 x 30 R_E domain.

The magnetotail is a critical volume of the Geospace environment that regulates the global circulation of magnetic fields and plasmas in response to changing solar wind conditions. In it, impulsive localized flow bursts are launched and dissipate, powerful electric currents form and evolve abruptly, and magnetic energy is explosively converted to particle energy. A fundamental plasma process known as magnetic reconnection is thought to be important to the most common form of “space weather”, the auroral substorm. These are recurrent energy releases that become more frequent during magnetospheric storms. The dynamism and turbulence of the magnetotail have humbled our efforts to observe and understand it using individual spacecraft. The magnetotail magnetic fields and plasmas do possess an underlying, slowly varying coherent structure, but strongly turbulent flows and fields are usually large compared to the background field or flow. Thus, globally coherent pictures of the system dynamics become lost in the “noise” of individual measurements. Despite over 30 years of research with ever more sophisticated instrumentation on ever larger and more complex spacecraft, fundamental questions concerning the structure and dynamics of the three-dimensional magnetotail remain unanswerable. Accordingly, scientific progress has stagnated. Intelligent, reasonable scientists cannot reach consensus on these issues, not for lack of models and theories, but because of a lack of the most relevant measurements. Neither current single spacecraft, nor even tight groups of spacecraft, are sufficient to resolve these theoretical controversies.

Magnetotail Constellation DRACO is guided by the following scientific objectives:

- Determine the *equilibria* of the magnetotail, revealing the actual instantaneous (versus statistical average) structure of the turbulent magnetotail.
- Understand the *responses* of the magnetotail to solar wind disturbances, resolving them from fluctuations that arise under steady solar wind conditions.
- Reveal the *instabilities* of the magnetotail, and differentiate them from direct solar wind responses that closely track conditions in the driver medium.
- Map the *linkages* between local and global processes, to trace the causality and energy flow from sources to sinks of mass and energy.

Magnetotail Constellation DRACO will provide the first global time-evolving maps of fields and flows in this important region. Using recently available technologies, the magnetotail can now be reached with a swarm of small spacecraft. Such a swarm is novel in its ability to simultaneously resolve magnetic fields and flows throughout large volumes of the magnetotail. Magnetotail Constellation DRACO is designed to provide the groundbreaking data needed to understand how the magnetotail really functions. It is responsive to the NASA’s Office of Space Science Sun-Earth Connection (SEC) theme’s strategic thrust: to understand solar variability and its influence on the Earth and the other planets.

Fundamental plasma transport and energy conversion processes in the magnetotail range in spatial size from the microscopic, kinetic regime, all the way to the largest global scales. NASA's STP's have been sequenced to explore these spatial ranges systematically. The Magnetospheric Multiscale (MMS) Mission will focus on the smallest-scale, microphysical processes occurring in and near magnetospheric boundary layers: magnetic reconnection, charged particle acceleration, and microscopic turbulence. MMS will provide unprecedented vision into the microphysics of these fundamental plasma processes, but these closely-spaced spacecraft will be unable to make observations simultaneously over scales ranging up to 10's of R_E. Accordingly, whereas MMS is the plasma physical "microscope", Magnetotail Constellation DRACO is strategically designed to be a "meso/macro-scope", extending our vision across the magnetotail as a complement to MMS. IT will resolve persistent controversies and lead us to an understanding adequate to serve as the foundation of a predictive science of magnetospheric meteorology.

To gain this unprecedented macroscopic view, Magnetotail Constellation DRACO will provide simultaneous multi-point measurements, resolving system scales down to 2 R_E over a 15 x 30 R_E domain, at time scales down to 10 sec. The measured magnetic and plasma flow fields will be used to track propagating fronts and disturbances in the magnetotail, construct time-dependent maps of large-scale current systems, develop synoptic maps of flows from their sources, and explore the global consequences of reconnection and other acceleration mechanisms.

Mission implementation consists of 100 *nanosatellites* (defined as ~10 kg mass or less) distributed in nested, near-equatorial orbits, all sharing a common low altitude (~3 R_E) perigee, with apogees ranging incrementally from 7 to 40 R_E. Primary mission science will be completed during several consecutive months each year as the coplanar orbits' common lines of apsides sweep through the magnetotail. Excellent ancillary science will be performed during the balance of the year when the constellation probes the dayside magnetosphere, magnetosheath, and solar wind regions. The nominal Magnetotail Constellation DRACO mission has an expected operational duration of two years. The launch is currently scheduled for 2010/2011, but could be advanced to mid-2008, depending on the overall robustness of funding for the STP line. The enabling technologies needed to implement DRACO are currently in place, or are in advanced stages of development, except in the area of (high-count) constellation fabrication and deployment technologies. The recently selected NASA Nanosatellite Constellation Trailblazer ST-5 mission will provide much of the spacecraft technological development and readiness needed for Magnetotail Constellation DRACO to successfully achieve its scientific goals. However, several enhancing technologies should be pursued vigorously and funded to foster launch readiness and provide for a more comprehensive scientific mission. These include but are not limited to: miniaturized magnetometer, plasma analyzer, energetic particles analyzer, and other possible measurement technologies; integrated "sciencecraft" systems design; advanced data synthesis and visualization techniques; and advanced techniques for multi-point data assimilation into global magnetospheric simulation models.

Features of Magnetotail Constellation DRACO:

- Supports *closure* of magnetotail controversies unresolved for in excess of 30 years for lack of required observations.
- Resolves space from time throughout the dynamic magnetotail system, providing first knowledge of magnetotail *equilibria*, *responses*, *instabilities*, and *linkages*.
- Single Delta launch creates constellation; with possible launch in mid 2008.
- 100 spacecraft at a mean nearest neighbor separation of ~2 Earth radii over 15 x 33 R_E domain.
- Primary science accomplished annually when the constellation sweeps through the magnetotail; Ancillary boundary science accomplished during balance of each year.

1. Scientific Objectives

1.1. Magnetotail Configuration

The geomagnetic field carves out a cavity in the flow of solar wind plasma, known as the *magnetosphere*. The deflected solar wind plasma streams away from the Sun along the outside of the *magnetopause*, the locus of positions where the incident solar wind pressure balances that of the geomagnetic field. A small fraction of the solar wind, mass, energy, and momentum enter the cavity, resulting in the formation of boundary layers streaming just inside the boundary. Some of the anti-Sunward moving plasma is drawn from the dayside magnetosphere, removing plasma from that region. A process known as magnetic *reconnection* enhances this removal of internal plasma, and removes magnetic field as well. Reconnection breaks open the closed geomagnetic field lines and "reconnects" each end of them to solar wind field lines, coupling and mixing the solar wind and internal plasmas. The motion of the solar wind drags the plasma on these field lines downstream. Later, open field lines must eventually reconnect a second time, decoupling their Earth-rooted ends from their solar wind end, and restoring them as closed field lines within the magnetosphere or in the solar wind.

Mixed internal and external plasmas that become trapped within the geomagnetic field and are unable to escape downstream, pile up in the magnetotail and then spread back toward the dayside magnetosphere from which it came. The external plasma that enters the closed field region must be slowed down and turned around to remain within the magnetosphere. The force to accomplish this is derived from the stretching of the magnetic field lines, behaving like rubber bands, into a long magnetotail. The stretching continues until some as yet undetermined instability occurs, which most likely involves reconnection. The extended magnetic field lines, and the plasma on them, then relax back closer to a dipolar configuration, often releasing a magnetic bottle of plasma, a *plasmoid*, into the downstream solar wind [Hoshino et al., 1996; Mukai,et al., 1996; Slavin et al., 1993; 1998]. While the stretching phase can be gradual, the relaxation toward a dipolar configuration is typically abrupt and dramatic. Energy stored in the stretched magnetic field is released and particles are energized, injected into the inner magnetosphere, and precipitated to form auroras at high latitudes. Geomagnetic activity increases, and seed populations are created that are further accelerated to form the transient radiation belts of the inner magnetosphere.

The Earth's magnetotail consists of several distinct regions as shown in *Figure* 1. Much of the plasma in the magnetotail is within the *plasma sheet*, a region of hot plasma extending across the tail from the dawn edge to the dusk edge, and extending from the distant tail into the inner magnetosphere. The pressure of the plasma sheet is substantial and supports the stretched field lines of the tail in a delicate balance, while separating the northern and southern *lobes*. These are regions of stronger magnetic field guiding supersonic *polar wind* outflows of plasma from the Earth's ionosphere, rushing into the relative vacuum of the lobes. The vacuum of the lobes results from the lack of Sunward streaming particles in the hypersonic solar wind and the action of reconnection, which allows plasma to escape rather than being trapped in the tail, beyond the reconnection site. Enshrouding the northern and southern lobes are regions of dense, cool plasma flowing along the magnetic-field lines in the antisunward direction: these are the plasma *mantles* or *High Latitude Boundary Layers* (HLBL), mainly solar wind plasma with a minor component of escaping internal plasma. On the dawn and dusk sides of the magnetosphere are the *Low-Latitude Boundary Layers* (LLBL), regions of antisunward flowing plasma of solar-wind origin, again mixed with some internal plasma. Finally, on the outer skin of the plasma sheet, adjacent to the lobes, are the northern and southern *Plasma-Sheet Boundary Layers* (PSBL). These typically contain magnetic-field-aligned beams of electrons and ions, that originate from trapping of the anti-Sunward lobe or mantle flows by magnetic reconnection farther down the tail.

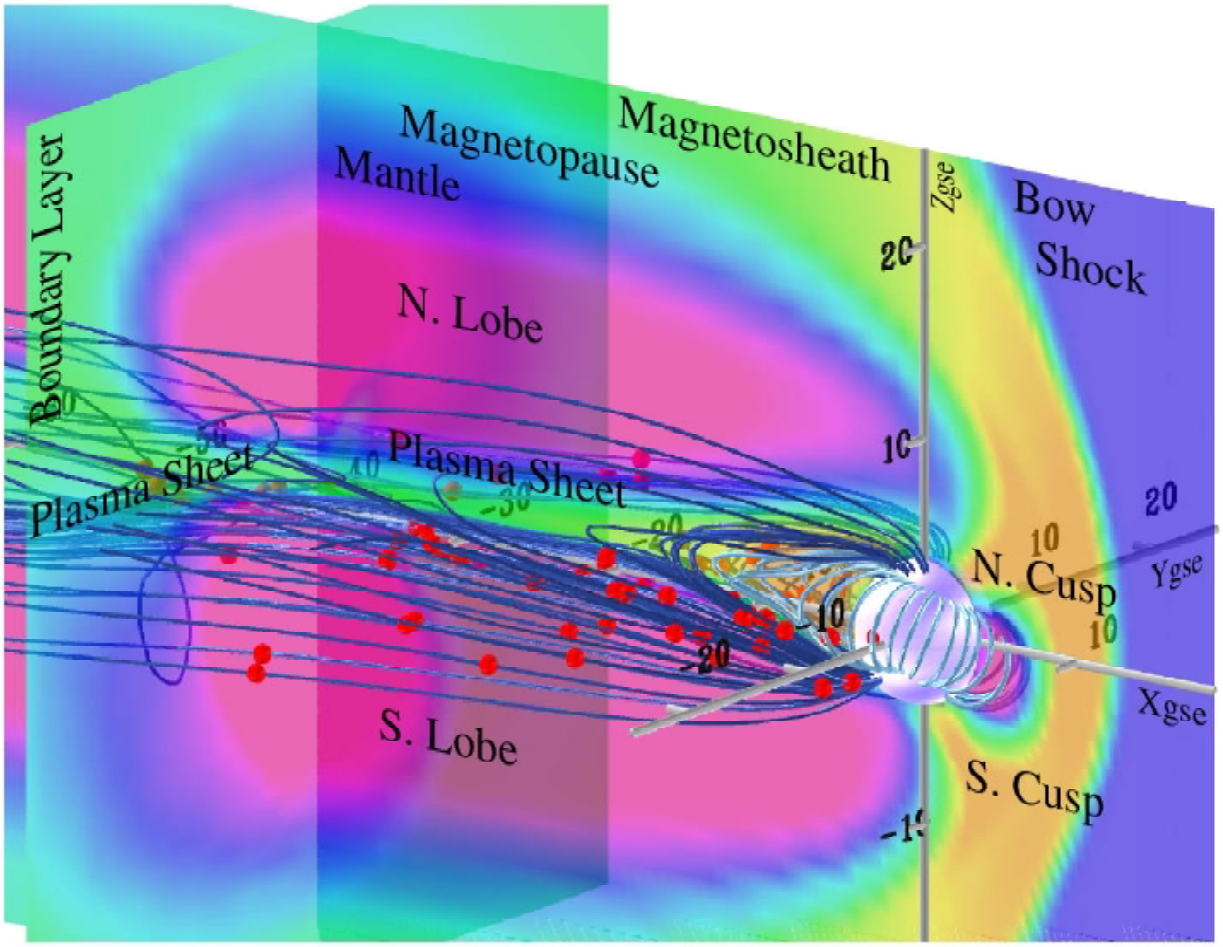

Figure 1. The computed magnetotail and its major component regions and boundaries in three dimensions, as illustrated by the by results from magnetohydrodynamic global simulation modeling. Color coding indicates plasma density on intersecting planes at Y=0, and at X=-40 Earth radii. Labels indicate significant boundaries and other features. Light blue magnetic field lines originate from geomagnetic mid-latitudes, while dark blue field lines originate in the polar cap region. Red dots indicate typical constellation spacecraft positions near the plasma sheet (green color on the Y=0 plane). Courtesy of J. Raeder/UCLA.

1.2. The Substorm Problem

The Earth's magnetotail is a complex and dynamic region of the magnetosphere. The large-scale flow pattern of the plasma sheet is typically concealed by intense small-scale plasma flows. The magnetic field in the plasma sheet often exhibits small-scale kinks and tangles. The Earth's magnetotail undergoes large changes in its global morphology during *substorms* and during *magnetic storms*. The magnetospheric research community relies on a conception of the magnetotail that is constructed by averaging measurements taken by various lone satellites and whose dynamics is studied by computer simulations with coarse spatial resolution and low Reynolds numbers. The community has come to realize that the deficiencies of of this magnetotail conception are impeding progress in understanding how the magnetosphere really works.

Ever since Syun Akasofu [1964] showed that auroral phenomena could be organized into characteristic recurrent patterns called “auroral substorms”, these substorms have been a topic of vigorous debate. There is broad consensus that the magnetotail exhibits a characteristic behavior known as a substorm, defined by diverse observed aspects including auroral expansion, magnetic field dipolarization, current wedge formation, dispersionless particle injections, bursty bulk flows, and current disruption [Raeder et al., 1997; Fairfield et al., 1998; Nagai et al., 1998]. There is, however, no consensus concerning the physics of substorms, as suggested by the persistence of a designation that is only useful for classification and conveys little understanding of physical basis. Recently, the debate has centered on the first few minutes of the substorm expansion phase, the so-called “substorm onset”. The first sign of substorm activity should be located close to the causative source. Two theories, each associated with a different initial location of substorm onset have been proposed.

One theory [e.g., Lui, 1991; 1996] holds that substorms start near or slightly outside geosynchronous orbit. Theories in this class suggest that the electric current that produces the stretching of tail field lines is disrupted from flowing across the tail, flowing down along magnetic field lines and through the ionosphere instead. This forms the “substorm current wedge” [McPherron, 1973], a transient substorm feature inferred from magnetometer measurements near geosynchronous orbit. The new current system allows the local magnetic field to relax and become more dipolar, launching a rarefaction wave that propagates down the magnetotail [Jacquey et al., 1993; Lopez et al., 1994]. Some 20-30 Earth radii down the tail, it initiates increased magnetic reconnection of the type that turns open lobe field lines back into closed field lines in the magnetosphere. This causes plasma to rush Earthward through the plasma sheet, allowing the plasma sheet to quickly reestablish itself and recover its plasma pressure and cross tail current.

The other theory [e.g., Schindler, 1974; Birn et al., 1996; Baker et al., 1996; 1997] argues that substorms start with increased in reconnection at a distance of 20-30 Earth radii. The stretched lobe magnetic field is reconnected, creating a burst of plasma flow that launches captured plasma and field toward the Earth, at the same time forming a plasmoid that is shed downstream [Slavin et al., 1993; 1998]. The Earthward burst launches a compression wave toward Earth [Moore et al., 1981; Reeves et al., 1996; Li et al., 1998], creating a flow that runs into denser plasma and stronger magnetic field and is slowed and deflected as a result. The braking of the flow creates the observed substorm current wedge, in this scenario.

Both of these theories seek to account for the characteristics of a substorm in the magnetotail, including the dipolarization (relaxation) of the magnetic field to a less stressed state, the substorm current wedge, and the acceleration and injection of plasma into the dipolar region. However, the two have completely opposite flows of causality, in one case from the tail toward the Earth, in the other from near the Earth out into the magnetotail. The difficulty lies in the localization of the phenomena both in space (1-2 R_E) and in time (10-20 sec). Single spacecraft within the vast magnetospheric system have little chance of being at the key region at the exact time of substorm onset. More importantly, the lack of simultaneous measurements from adjacent “pixels” of this vast system prohibits placing the observed phenomenon in the context of the global magnetotail evolution. Many simulation results support to the idea that the initial substorm disturbance originates farther out in the magnetotail and then propagates inward as described above in the second theory. Limited observations [Ohtani, 1988] show that the field configuration changes propagate inward in a speed less than the sound speed, suggesting that they are not accomplished by a hydromagnetic compression wave. Other observations suggest that the changes are simply convected by fast plasma flows (100s km/s), but field configuration changes were observed to travel as slowly as 25 km/s from 6.6 R_E to 4.5 R_E. Lack of consistent observational confirmation indicates that neither theory can be

declared false or accepted as definitive. Thus, the most prevalent and important physical process in the magnetotail continues to escape scientific identification.

1.3. The “Quiet” Plasma Sheet Problem

In addition to the above substorm quandary, we also have a poor understanding of the quiet time behavior of the magnetotail. Single-satellite observations have presented glimpses into the underlying texture of the near-Earth magnetotail. It is known that the magnetic field of the plasma sheet has large fluctuations and that its plasma flows are highly erratic [e.g., Hayakawa et al., 1982; Borovsky et al., 1997]. Statistical treatments reveal an average Earthward flow in the plasma sheet, but with fluctuations as large or larger than the average flow, as shown in *Figure* 2. Short-lived, high-velocity “bursty bulk flows” were observed [Baumjohann et al., 1990; Angelopoulos et al., 1994], and they appear to be a significant if not dominant part of the long term average transport. This irregular flow of the plasma sheet may at times be fully turbulent. Turbulence data-analysis methods have been applied to single-satellite measurements of fields and flows [Borovsky et al., 1997]. Models of the magnetotail morphology based upon turbulent transport have been developed, and models of auroral activity driven by flow turbulence in the plasma sheet have been constructed [Swift, 1981; Song and Lysak, 1988]. Present estimates for the important spatial and temporal scales in the plasma sheet are about ~2 R_E and ~10 sec for flow bursts, and a few R_E and a few minutes for flow eddies and magnetic-field structures.

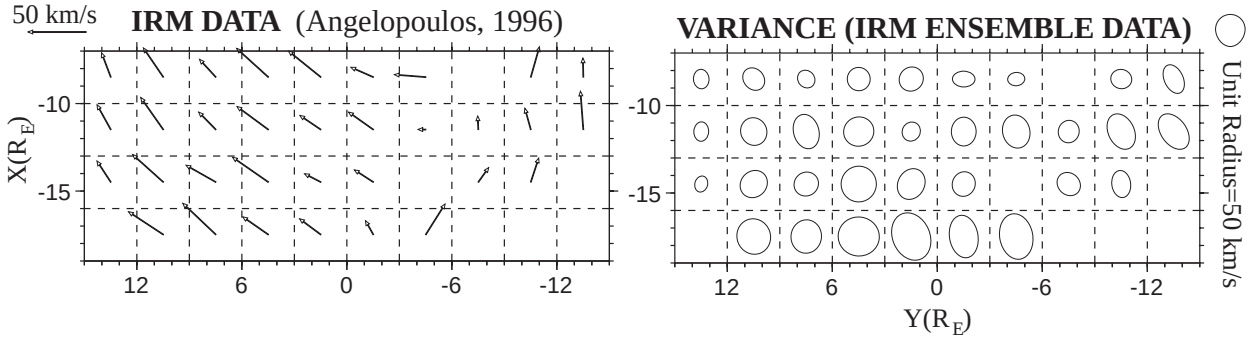

Figure 2. The mean flow and variability of the magnetotail, showing that a Sunward/duskward circulation prevails (in the positive X and Y directions), but that the variability of the flow is as large or larger than the mean flow speeds (right panel). Courtesy of V. Angelopoulos.

1.4. Science Objectives and Questions

The issues to be resolved can be distilled down into a concise list of specific objectives for Magneotail Constellation DRACO, with questions to be answered, as follows:

1.4.1. Determine the *Equilibria*

Are there any equilibria of the magnetotail? Is there a persistent reconnection region in the tail, for quiet and steady solar wind? What are its properties and how does it depend upon the pressure, speed, and magnetization of the solar wind? Does magnetotail flow fluctuate strongly even when the solar wind is steady? How do these fluctuations depend on the pressure, speed, and magnetization of the solar wind?

Simultaneous observations of the entire plasma sheet during steady solar wind conditions will make it possible to identify both the equilibrium state and its fluctuating component.

1.4.2. Understand the *Responses*

How does the magnetotail respond to abrupt changes in solar wind conditions (e.g., the crossing of a high speed stream boundary including standing shocks; to the passage of a travelling shock wave; to a magnetic cloud generated by a coronal mass ejection event? Are large-scale flow vortices generated in response to solar wind disturbance? Can the shedding of a plasmoid be triggered by solar wind variations?

Knowing how the magnetotail is configured during steady conditions, we will be able to recognize unambiguously its unique response to characteristic discrete solar wind disturbances.

1.4.3. Reveal the *Instabilities*

Where, when, and with what shape do reconnection regions form in the plasma sheet? Recent global simulations suggest that sinuous narrow channels of high-speed flow are sporadically formed in the near-Earth plasma. How are these flows launched and dissipated? Bursty bulk flows are observationally associated with the relaxation, also called dipolarization, of tail magnetic field stretching. But dipolarization implies the disruption of current systems that support the tail. How are the current systems related to plasma flows and acceleration? How are they related to auroral substorms and plasma injections? Are the bulk flows or current disruptions, the same disturbances that shed plasma and magnetic field lines from of the magnetotail in structures known as plasmoids?

Magnetotail Constellation DRACO will for the first time clearly identify internal instabilities of the magnetotail. It will determine their threshold conditions, and ultimately allow us to understand and predict their occurrence.

1.4.4. Map the *Linkages*

When the tail equilibrium is disrupted by either internal or external disturbances, where does the process begin, and how is its action communicated to other parts of the magnetosphere? Are there different categories of disruptions with different sequences of development? Dynamic plasma systems like the magnetosphere are known to be coupled by hydromagnetic or plasma waves. On slower time scales, changes are transported convectively from initiation to destination. However, propagation of waves or flows is impossible to follow using a single or even a group of spacecraft.

DRACO's extended measurement grid will depict clearly the propagation of waves or vortices through the magnetotail, revealing the flow of cause-to-effect for the first time. DRACO measurements will also identify plasma sheet conditions of flow and magnetic shear within which microscale transport processes such as reconnection are important, complementing microscale measurement missions such as Magnetospheric Multiscale (MMS).

In summary, the overarching goal of the Magnetotail Constellation DRACO mission is to resolve issues of magnetotail physics that have plagued magnetotail studies for over 30 years, centering around magnetotail *equilibria, responses, instabilities,* and *linkages*. To achieve observational closure with theory-based simulations, leading to confidence in our physical description, we must observe the plasma sheet system as a whole, from ~ 7 to

~40 R_E in the tail. This requires an array of measuring stations dense enough to resolve features ≥ 2 R_E in extent, during characteristic dynamic episodes having shortest time scales ≥ 10 sec in duration.

1.5. Motivations and Unique Aspects

1.5.1. Lessons Learned from Dynamic Atmospheric Meteorology

Earth's magnetosphere is a complex geophysical system formed by interactions between the supersonic solar wind and the plasma and gas atmospheres of the Earth. It is certainly valid and increasingly common to think of the magnetosphere as a part of the Earth's overall weather machine [Calder, 1974]. "Weather" may be defined simply as the cosmic dynamical phenomena that are of interest to humankind by virtue of their occurrence within space that we inhabit. Increasingly, we inhabit the space around the Earth out to the limits of our atmosphere and beyond, into the atmosphere of our star, the Sun. We also invest in the placement of robotic agents within that space, whose survival is important to us for various practical reasons. Thus, magnetospheric phenomena are beginning to have relevance to our lives and are becoming more familiar to us in this space age.

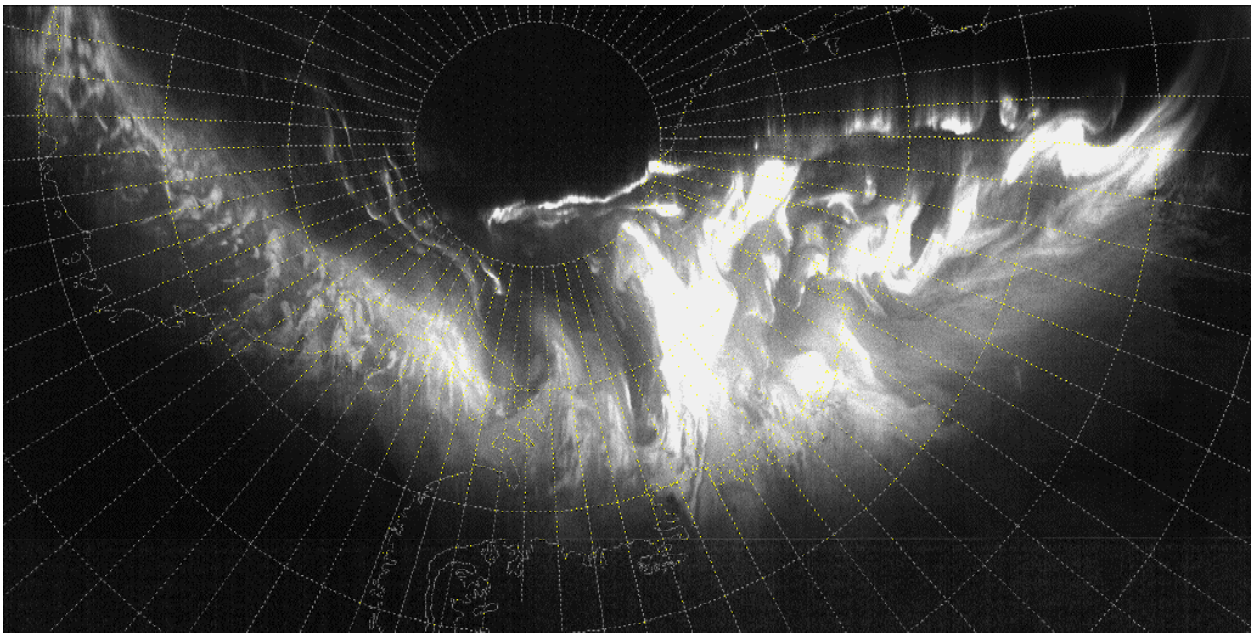

Figure 3. An example of the global auroral structure during a significant magnetospheric disturbance. This image is courtesy of the Air Force Research Laboratories and was acquired in a stripwise fashion as the Defense Meterological Spacecraft Program (DMSP) spacecraft moved along a relatively low Earth orbit.

The electrical conductivity of plasmas, and the resultant importance of electromagnetism, distinguishes the magnetosphere from the lower atmosphere of Earth. Its magnetization leads to behavior that is unintuitive, even for scientists and technicians with extensive training in atmospheric gas dynamics. The polar aurora, usually considered to be a two-dimensional image of the plasma sheet, complicated by electrodynamics processes within it, is a good example. No other commonly experienced gas flow generates electrical discharges leading to enhanced luminescence of the flowing gases (with the possible exception of tornadoes). Yet a single view of the global aurora

in this context suggests strongly that it is fundamentally a turbulent fluid flow phenomenon, as shown in *Figure* 3. The global structure of the polar aurora is quite comparable to that of the global cloud cover of our planet, as exemplified in *Figure* 4. Clouds and aurora both provide telltale identifications of fluid parcels with distinguishing characteristics of moisture content and particle precipitation, respectively. As these parcels are transported and distorted, they reveal much about the flow patterns that exist within their parent fluids. Both of these figures reveal the presence of large scale eddies and vortex flows, a conclusion that is reinforced when time-lapse motion pictures of these phenomena are viewed.

The modern account of global winds derives from the work of meteorologists over the past two and a half centuries. In the words of Nigel Calder [1974], “above all, the modern account is based on millions of measurements of conditions high over our heads, made by balloons, aircraft, and satellites”. In combination with the theoretical work of Rossby, Starr, Charney, and Lorenz (some of which lead to a more general theory of chaos), and their working computer models of global circulation, a high level of understanding has been reached. Terms like jet stream, front, depression, pressure ridge, and even baroclinic instability, have entered the vocabulary of the general public through daily discussion by news media weather forecasters everywhere.

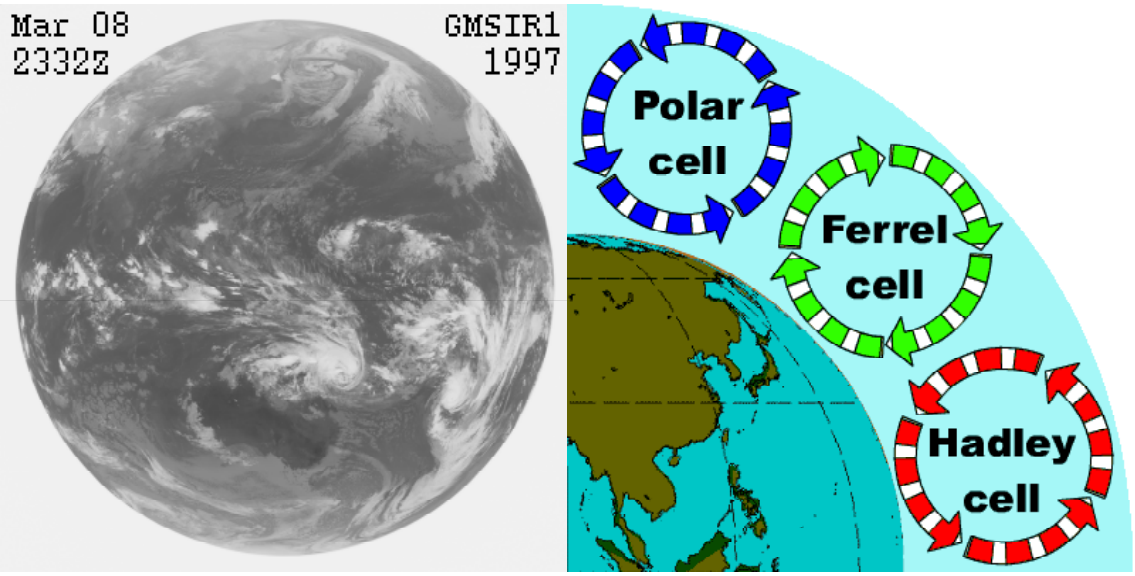

Figure 4. (Left Panel) An example of Earth’s global cloud cover imaged in visible light, illustrating the complex circulation of our atmosphere in response to the flow of heat from equator to pole, the baroclinic instability. (Right Panel) Mean meridional atmospheric flow, owing to the breakup of the equator to pole cell proposed by Hadley, into three cells, leading to the formation of the Ferrel cell and mid-latitude weather. Figures courtesy of the University of Washington Geophysics Program.

In the troposphere, planetary rotation sets up a balance between the pressure and Coriolis forces, stabilizing against planet-wide Hadley convection, or thermal overturning of the atmosphere. However, the thermal conductivity of the atmosphere is insufficient to support the available energy flux. To move more heat from the equator to the poles, the system develops a baroclinic instability whose circulation permits the energy flux to be transported convectively, albeit in a complex 3D pattern involving a mid-latitude overturning cell in addition to polar and equatorial cells. The mean meridional motions (in latitude) are illustrated in *Figure* 4. Superposed on these mean motions are the frontal and storm phenomena that make up mid-latitude weather. Sustained global and local monitoring of weather

conditions, combined with sound theoretical underpinnings, have permitted weather prediction to become usefully accurate over time scales of up to a week or two, though useful climate predictions continue to elude us at present.

Magnetospheric meteorology is on a trajectory similar to that of tropospheric meteorology. Pioneering thinkers such as Dungey, Axford, Hines, and Nishida developed the basic description of the overall circulation of the magnetosphere. Corresponding to the Hadley cell for the magnetosphere, this model of magnetospheric circulation gets the overall pattern correct, but overlooks much of the important and interesting dynamics. It was realized almost immediately [Dungey, 1966; McIlwain, 1967; see acknowledgements] that further progress on global dynamics would be limited with individual observing station (spacecraft) data. They recognized that literally "bunches" of spacecraft would have to be put in orbit to definitively understand the local and dynamic behavior of the magnetotail and its aurora plasmas. Since that time, considerable theoretical work has been accomplished and indeed, numerical models have been constructed of the magnetosphere and its dynamics, as exemplified in *Figure* 1. Nevertheless, the very small number of multi-point simultaneous measurements has greatly hampered closure between models and observations. The true behavior of the magnetosphere eludes us and we have many competing theoretical ideas with no way of refuting most of them. Consequently we have an unrelenting debate, and a poor basis for understanding and predicting magnetospheric dynamics.

The magnetosphere has many storm-like departures from the mean expected circulation. The basic driving force, analogous to the thermal driving of the troposphere, is the solar wind flow, which seeks to impart momentum to the outer layers of the magnetospheric plasma. The large cycles of magnetotail distension and collapse suggest an instability that might be called "barotensile" in recognition of the disruption of balance between plasma pressure and magnetic tension. This is loosely analogous to the disruption of a balance between pressure gradient and Coriolis force in the baroclinic instability. The net result is that some parts of the tail plasma are carried off downwind, while other parts convect rapidly toward the Sun through the inner magnetosphere. The instability allows greater transfer of momentum through the system, analogous in some ways to the convective spreading of heat energy by the baroclinic instability. A comparison of the baroclinic and barotensile instabilities is summarized in **Table** 1.

Table 1. Parallels between the baroclinic instability and the magnetotail's barotensile instability

Category	**Baroclinic Instability**	**Barotensile Instability**
Driver:	differential heating	shear flow
Object	heat transport	momentum transport
Obstacle	low conductivity	low viscosity
Mechanism	3D convection	3D reconnection
Disequilibrium	pressure gradient vs. Coriolis force	pressure gradient vs. Maxwell tension

Just as the true nature of the baroclinic instability emerged from millions of measurements of conditions throughout the troposphere, the true nature of magnetospheric global instabilities responsible for auroral substorms and storms will come from a program to obtain simultaneous global measurements. This will lead to a more complete understanding of the Sun-Earth system and eventually the capability to predict its behavior over longer time spans. We now need observations with a resolution in time and space that is commensurate with our knowledge of correlation scales in the plasma sheet, and of hydrodynamic wave propagation times across such scales: 2 R_E and 10 seconds. To achieve this, we must develop affordable means by which conditions can be measured at many points simultaneously and repetitively, and integrate them into space weather maps. This is the goal of Magnetotail Constellation DRACO (and all other constellation missions).

1.5.2. Hierarchy of Scales and Mission Architectures

The progression from single satellites to constellations is driven by the hierarchical nature of magnetospheric phenomena. Spatial scales of magnetospheric phenomena range from kinetic scales associated with magnetic reconnection to whole-body (i.e., magnetosphere-wide) responses to solar wind waves and discontinuities. Associated with the hierarchy of spatial scales is a hierarchy of temporal scales, since large-scale phenomena tend to last longer than small-scale phenomena. Moreover, the scales are interrelated; one scale feeding into the next and vice versa.

The hierarchical nature of magnetospheric phenomena exemplifies a general property of astrophysical plasmas. T. Tajima [1997] remarks that the "hierarchical nature of plasma manifests itself as a kind of structure made up of levels of physical phenomena. But these are yet ultimately interrelated to each other." He illustrates the point with the example of magnetic reconnection, a local process that occurs as a result of global dynamics and in turn gives rise to global dynamics.

Meteorological phenomena also exhibit a hierarchy of scales, which feed into each other. The analogy to meteorology helps explain why magnetospheric physics must advance by progressing from single satellites to constellations. Meteorology is an older field than magnetospheric physics. It has approached the problem of understanding atmospheric phenomena by formulating the equations of motion of the atmosphere and developing an observational procedure for measuring the terms that enter these equations. The most important of the dynamical terms are wind, pressure, and temperature. For the most part, these quantities are invisible in the sense of being inaccessible through remote sensing. Meteorologists have found that the way to advance in the face of a hierarchy of dynamical scales driven by invisible forces is to establish an *in situ* observing network. The meteorological observing network has grown to become dense enough and broad enough to display atmospheric phenomena in the dynamical parameters—wind, pressure, and temperature—on all relevant scales. It is also broad enough to be able to follow weather-producing atmospheric phenomena through their life cycles. To achieve an adequate network, meteorology moved from single isolated stations to networks in which the number of nodes grew to encompass the phenomena.

Magnetospheric physics is in a closely analogous situation to meteorology with hierarchical dynamical modes and invisible dynamical parameters, which in this case include also electromagnetics. In this type of situation, the problem of data-theory closure has no known solution other than that developed in meteorology—a dense, broad network of in-situ observing stations. In the magnetospheric context, this means moving from single satellites to networks of satellites—single satellites, then clusters, then constellations—until the magnetosphere itself is encompassed.

Figure 5 schematically illustrates the hierarchy of magnetospheric scales and how these scales relate to classes of missions. The axes in the figure are characteristic size and characteristic duration. Characteristic size is divided into microscale, mesoscale, macroscale, and global. These are deliberately vague to allow many phenomena to be included. "Microscale" roughly represents kinetic (non-magnetohydrodynamic) processes. "Mesoscale" represents phenomena that have scales sizes roughly between an order of magnitude bigger than the microscale and an order of magnitude smaller than the scale sizes of the internal structures of the magnetosphere. "Macroscale" represents phenomena that have scale sizes comparable to the internal structures of the magnetosphere. "Global" phenomena engage the whole magnetosphere. Scales for duration are represented by phenomena having those durations. Roughly speaking, "Kinetic" corresponds to durations less than several seconds, "ULF" to durations from several

seconds to several minutes, “Advection” from several minutes to 10s of minutes, “Drift” from 10s of minutes to an hour or so, “Convection” from an hour or so to multiple hours, “Charge Exchange” from multiple hours to a day, and “Diffusion” anything longer than a day. As phenomena, these designations actually overlap, but they help to order the items on the plot.

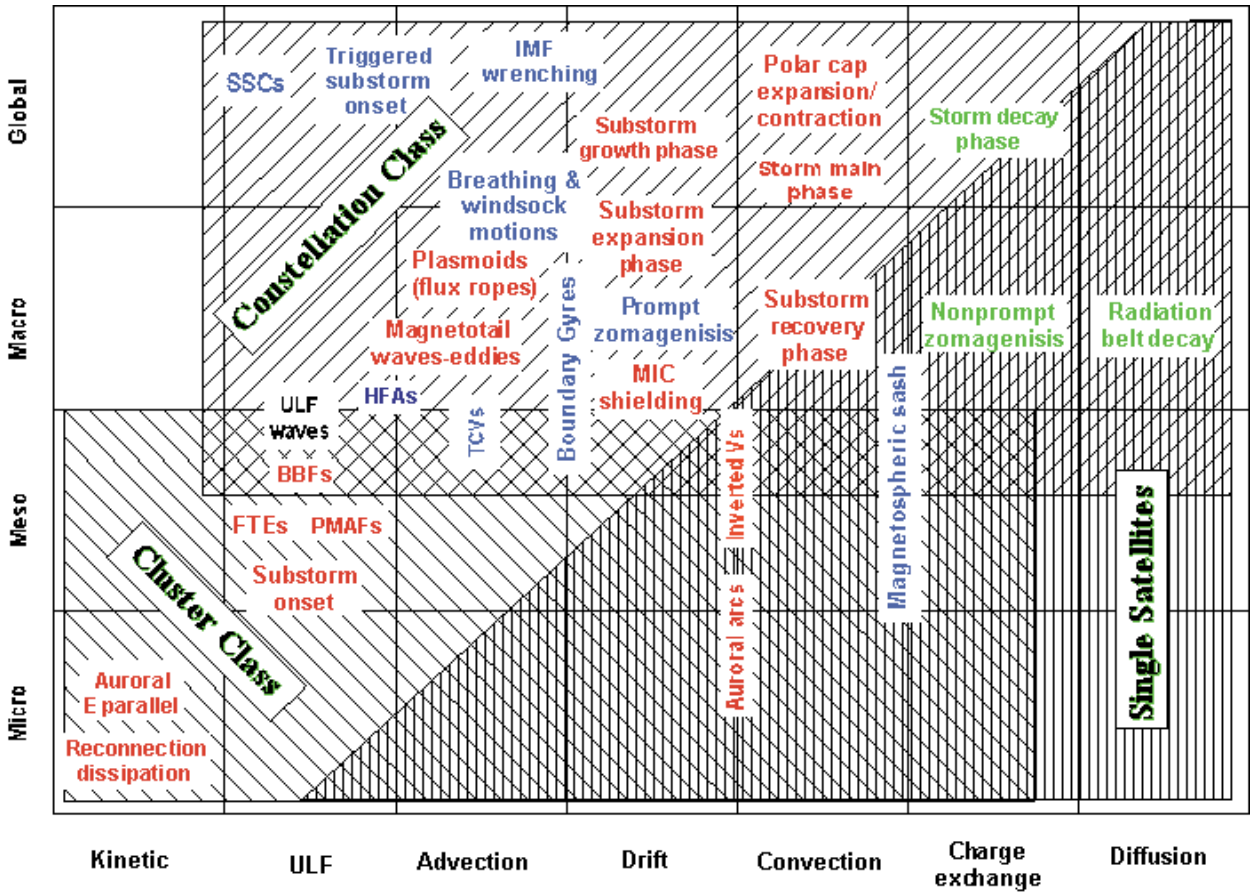

Figure 5. Hierarchy of scales in the magnetotail. Figure courtesy of G. Siscoe.

The phenomena are color-coded to represent mode of origin. Blue designates phenomena that arise from sudden solar wind and IMF changes. Red designates phenomena that arise from magnetospheric convection. Green designates diffusive phenomena. ULF phenomena are in black because they arise from multiple causes. To explain each entry would take a textbook in descriptive magnetospheric science, which is not warranted here. The point is that all scale sizes and durations are represented. Moreover, phenomena at different scale sizes are related by mode of origin. Convective phenomena cover all scales, and solar-wind-change phenomena cover nearly all scales. This illustrates for the magnetospheric case the point that Tajima made about astrophysical plasmas in general, they are hierarchical and their scales relate to each other.

Three classes of missions—single satellites, cluster class, and constellation class—are indicated by hatched regions. The areas included in each region are approximate. The region covered by “Single Satellites” corresponds to satellites with about a 15 Re orbit. The distance scale and the duration scale are then set by how far the satellite goes in a given duration. The region marked “Cluster Class” covers microscale and mesoscale phenomena of all

durations. “Constellation Class” missions cover macroscale and global scale phenomena of all durations. They also cover the upper size range of mesoscale phenomena, including Bursty Bulk Flows (BBF).

Consider now what each class of mission provides. Single satellites can describe the state of phenomena that change very slowly, such as the relatively slow moving magnetospheric boundary layers, inverted Vs, and diffusive changes in the ring current and radiation belts. For other phenomena, single satellites can only give statistical information accumulated by multiple encounters with the phenomena on separate occasions. In meteorological terms, for other phenomena single satellites give climatologies rather than descriptions of actual weather systems.

Cluster missions can describe the state and evolution of the microphysics of reconnection events, double layers in auroras, the local explosion that ignites substorms, and, at the magnetopause, Flux Transfer Events (FTE) and the correlatives of Poleward Moving Auroral Forms (PMAF). At the upper end of their range, they can capture appreciable pieces of BBF phenomenology, ULF waves, and, in the outer regions, the correlates of Traveling Convection Vortices (TCV), and Hot Flow Anomalies (HFA).

But most phenomena lie in the constellation domain. There are too many entries here to recite them individually. Especially to be noted are the red entries. These include the magnetosphere’s best known and most energetic dynamical modes, the substorm expansion phase and the magnetic storm main phase. Other entries include manifestations of flux ropes, turbulence, and waves, which are magnetospheric exemplars of universal plasma traits. These phenomena represent accessible examples of their class, the study of which constellation missions can tremendously advance.

In summary, the hierarchical, interdependent phenomena of astrophysical plasmas in general and of magnetospheric plasmas in particular drive a progression from single satellites to constellations. Meteorology has similar dynamics and has implemented a corresponding progression of atmospheric observing stations. Magnetospheric physics has passed through a single-satellite stage and is on the brink of a cluster stage. The time is right to plan for the constellation stage.

1.5.3. Data Synthesis Considerations for Constellation-Class Missions

Novel Modeling, Data Handling and Assimilation Techniques: The Magnetotail Constellation DRACO Mission will provide multi-point *in situ* measurements of the magnetosphere of substantially different quality and quantity than any previous mission. The quality of the measurements lies not so much in the quality of the individual measurements -- which are indeed comparable to previous missions -- but in the fact that these observations are made in a coherent fashion on a large number of spacecraft simultaneously. Making optimal use of the measurements will require the development and application of new techniques. The implementation of the DRACO Mission will result in a leap, similar in its importance to that made by the atmospheric physicists two hundred years ago. Individual weather observations were gathered into *synoptic* maps (summarizing a large number of individual observations). Later, the maps came to be further processed using spatial objective analysis and data assimilation. The analysis of individual spacecraft observations will become mostly obsolete and will be replaced by synoptic analyses that use observations from all satellites in the constellation. Techniques developed for the atmospheric sciences over the past decades can be borrowed to solve the new analysis challenges. This is critical for the success of DRACO because -- as the atmospheric sciences show us -- the development of these techniques can take decades and sometimes lead into dead ends. By exploiting the existing knowledge DRACO will make these tools ready for the first magnetospheric multi- point mission in less than a decade. It is crucial for DRACO's success to include a

strong modeling element right from the beginning. These analysis and assimilation tools need to be ready when the first DRACO measurements become available. The development of these tools will require substantial effort.

Data-based reconstruction of the evolving magnetosphere: It is difficult to understand the complex pattern of phenomena in the nightside magnetosphere without knowledge of the configuration of the magnetic field and its behavior in response to changing external conditions in the solar wind. One of principal goals of the modeling effort in the DRACO Mission is to develop reliable tool for reconstructing and visualizing the instantaneous magnetic field pattern on a global scale, using simultaneous data from the widely dispersed constellation of spacecraft. The approach is to represent the total magnetic field as a flexible combination of the partial fields from several model sources, having different spatial scales, and then fit the entire model field to the vector data, as downloaded from the "flying observatory" of the magnetometers. The resulting best-fit model of the global magnetic field will then allow one to reconstruct the instantaneous "snapshot" of the entire magnetotail. Combining the patterns derived at regular intervals of time will make it possible to trace the evolution of the global field, understand its relation to the dynamics of the plasma flows, and reveal the causality of the solar-terrestrial events. The success of such data-based magnetic mapping crucially depends on at least two factors.

The first factor is the simultaneous data coverage of the magnetosphere. A significantly non-uniform distribution of the satellites will result in a loss of information in regions with sparse coverage, while an excessively dense concentration of the space probes in relatively small regions will not enhance the fidelity because of limited spatial resolution of the mathematical models. Therefore, the inversion methods must include a means of "filling in the gaps"; for example, using the predictions of the global statistical models in regions with poor spatial coverage. Similar principles have been successfully applied in consolidating multi-point ionospheric measurements in the Assimilative Mapping of Ionospheric Electrodynamics (AMIE) models. In this regard, simultaneous monitoring of the conditions of the incoming solar wind could greatly enhance the accuracy of the DRACO-based modeling. In spite of the fact that the DRACO measurements will be made mainly at low latitudes, the dynamic evolution of the orbits and distortions of the tail will provide sufficient information about structure normal to the orbital plane [Tsyganenko et al., 1998].

The second factor is the flexibility of the model representation, that is, its ability to reproduce a large variety of possible magnetic configurations. Substantial progress in this direction has taken place recently. A mathematically simple and general approach was developed to model the largest-scale geomagnetic field, produced by currents on the magnetospheric boundary. This magnetopause contribution is important throughout the magnetosphere and depends mainly on the dynamical pressure of the solar wind. The cross-tail electric current, flowing from dawn-to-dusk in the equatorial plasma sheet, is also critically important. The most recent mathematical models [e.g., Tsyganenko and Peredo, 1994], superpose the fields from several equatorial current sheets with variable thickness and different radial profiles, all confined within a magnetopause with realistic shape and size. In addition, powerful new techniques became available recently, making it possible to take into account the seasonal/diurnal warping of the tail current and its twisting around the Sun-Earth line, induced by the reconnection of the geomagnetic and interplanetary magnetic fields [Tsyganenko et al., 1998]. Now many more degrees of freedom can easily be introduced into the model, making it possible to magnetically map the effects of catastrophic reconfigurations of the magnetotail during disturbed periods. Further progress in this area is expected on the basis of the new deformation method [Tsyganenko, 1998], allowing one to greatly expand the variety of modeled magnetic configurations, including plasmoids and other transient features.

Data assimilation in dynamic MHD modeling: Data assimilation takes the synoptic mapping a significant step further by introducing the "first principle" dynamical MHD models into the analysis process. The underlying idea is that assimilation of data can minimize errors in both the data and the model, even when the model suffers from simplifying assumptions, and thus provide an optimal "map" of the physical state of the magnetosphere at any given time.

Data assimilation techniques have been successfully used in atmospheric and oceanographic models for some time [Ghil et al., 1997] but never before in magnetospheric modeling. Data assimilation techniques take the observations distributed in time and space and merge them dynamically into the numerical model in order to determine as accurately as possible the instantaneous state of the magnetosphere. The primary objectives and needs for the data assimilation are our poor knowledge of the initial state that is used to start a model simulation and the fact that the simulated magnetosphere may gradually diverge in time from its actual state. Data assimilation ensures that, in the course of time, the state of the simulation remains optimally close (in terms of a merit function) to the concurrent observations at the measurement points. The primary reason that data assimilation methods have not yet found their way into magnetospheric modeling is the scarcity of magnetospheric in situ measurements. The Magnetotail Constellation DRACO Mission will change that dramatically by providing for the first time a fairly dense grid of *in situ* data describing the MHD state of the entire modeled system. The fact that these observations are restricted to the vicinity of the tail plasma sheet is no major obstacle. Atmospheric models have to deal with similar unevenly distributed data sets and powerful methods exist to make optimal use of them [Miller et al, 1994; Talagrand, 1997].

The power of data assimilation has been demonstrated convincingly by the numerical weather prediction models which all use assimilation techniques. Employing these techniques in magnetospheric modeling will result in a dramatic breakthrough, since the data assimilation will serve as an ultimate test of the underlying model's quality. A systematic divergence of a model from the data will provide a clue to some intrinsic deficiency to be corrected. In addition, not only will the model improve overall, but also new knowledge will be gained about the physical processes, whose incomplete or wrong description had caused the model to fail. In short, the data assimilation forces a continuing re-evaluation of our understanding of how the magnetosphere works. This is one of primary reasons why the DRACO Mission should be implemented.

1.6. Complementarity with Other Missions

NASA Sun-Earth Connection (SEC) missions are coordinated to provide knowledge about the magnetosphere at all relevant scales. The International Solar Terrestrial Physics (ISTP) missions provided the most global coverage to date, establishing the importance of continuous solar and solar wind monitoring in conjunction with single-spacecraft observations at other strategically-chosen locations. In the process, ISTP has also demonstrated the capability to remotely sense and image the energetic ions of the inner magnetosphere [Henderson et al., 1997, Jorgensen et al., 1997]. Soon, the IMAGE and TWINS Missions will put in place the tools for routine dedicated imaging of the inner magnetospheric energetic ions as well as the cold plasmaspheric helium, low energy ionospheric outflows, and the motions of the dayside magnetopause. However, imaging missions are unable to probe the magnetotail region, owing to the very low plasma and neutral gas densities in that region. Even with increased sensitivities, magnetospheric imaging missions cannot make vector measurements of the magnetic field and plasma flow field, being limited to scalar quantities such as line-of-sight flux. These are extremely important in the magnetotail region.

The five-spacecraft Magnetospheric Multiscale Mission (MMS) will focus upon the microscale processes that occur in magnetospheric boundary layers, including the thin magnetotail current sheet: reconnection, particle acceleration, and turbulence. These processes regulate the flow of mass, energy, and momentum from magnetotail lobe storage regions into the inner magnetosphere and ionosphere via high-speed plasma flows, energized particles, and field-aligned currents, thereby determining when and where geomagnetic disturbances will occur. Magnetospheric Multiscale will discriminate between spatial and temporal phenomena and provide the local gradient observations needed to characterize and then identify these poorly understood microscale processes.

The four-spacecraft Geospace Electrodynamics Connection (GEC) mission will define the nature of the connections linking the magnetosphere and the ionosphere. The key objectives of this mission include: i) identifying the spatial and temporal scales over which the ionosphere and thermosphere respond dynamically to magnetospheric input, ii) establishing the route linking magnetospheric and ionospheric currents as a function of conductivity, and iii) defining how plasma flows between ionosphere and magnetosphere affect the dynamics of both regions.

Whereas the MMS and GEC Missions will provide a wealth of information concerning the small-scale structure of processes in magnetospheric boundary layers and the ionosphere, neither mission will explore the global equilibrium, response to disturbances, and macroscopic instability of the magnetotail, nor its global linkages. These are questions that DRACO is designed to address, to complement the other STP missions.

2. Mission Requirements

2.1. Introduction

This section provides a derivation of Magnetotail Constellation DRACO science requirements from the stated scientific objectives. DRACO represents a significant departure from the established use of single or groups of spacecraft to measure local conditions or gradients. It follows directly that if a constellation mission shall be constrained to conventional resource allocations, it will require unconventionally small resource allocations for any single spacecraft in the constellation. Nevertheless, it makes no sense to deploy a constellation mission under such constraints unless the resources available are sufficient to provide for high-quality, focused measurements. The art of designing a constellation mission then clearly lies in the definition of the minimum instrument package per spacecraft, consistent with achieving the science objectives of the mission. In place of a single or small cluster of spacecraft armed with a wide variety of measurement devices, we shall instead be describing a mission wherein a very large number of spacecraft are equipped with a Spartan but effective instrument complement. Consequently, we deal first with the minimum required instrument payload, implicitly prioritizing a maximal number of spacecraft.

2.2. Measurement Requirements

The science objectives for DRACO are expressed in terms that identify the most fundamental measurements: magnetic field, plasma flow field, and energetic particle acceleration. These are the basic three measurements that DRACO will require. It may be objected that charged particles are accelerated by electric fields, so that electric field measurements are required as well. However, at the time scales of interest to DRACO (≥ 10 sec), and in the region of interest to DRACO, the electric field may be inferred from the plasma flow (transverse component) and from measurements of magnetic field variations (parallel component). Shorter time scale phenomena can usually be best observed using electric field measurements to integrate instantaneously over the plasma velocity distribution. However, such phenomena are declared to be beyond the scope of DRACO and can be best diagnosed by missions devoting their resources to detailed microphysical observations. **Table** 2 provides a compact summary of the measurement requirements for DRACO. A translation of these requirements into a straw man payload is provided below.

Table 2. Measurement Requirements

Measurement	Range	Resolution	Time Resolution	Comments
3-Axis Magnetic Field	+/- 300 nT	0.1 nT	1 sec 1min @ 100 Hz	Fluxgate technology exists
Plasma 2-D Temperature	10 - 20000 eV	20%	10 sec	Requires 180° field-of-view
Plasma Flux	10^2 - 10^8 cm^{-2} s^{-1} sr^{-1} eV/eV	20%	10 sec	Electrostatic analyzer technology exists
Plasma 3-D Velocity Electron PAD	1 - 1000 km/s	20% 20°	10 sec	Mass analysis significant but not absolutely required.
Particle Energy	20 - 500 keV	20%	10 sec	Mass analysis significant but not absolutely required.
Particle Flux	1E0 - 1E6 cm-2 s-1 sr-1	20%	10 sec	Solid state telescope technology
Particle Pitch Angle	180°	20°	10 sec	

2.3. Mission Requirements

2.3.1. Orbit-Attitude Requirements

Orbit: DRACO must sample the magnetotail region from about 7 R_E to 40 R_E in the nightside along the Sun-Earth line, and across the magnetotail east and west of the Sun-Earth line by ~10 R_E. This is based on the importance of phenomena within the region from geosynchronous orbit to beyond the convection reversal associated with substorm activity, near 25-30 R_E. Eccentric orbits with perigees near 2-3 R_E are required for economical transmission of commands and data. A set of orbits with apogees ranging from 7 to 40 R_E would provide all the coverage that is needed. The number of spacecraft required must be determined on the basis of detailed orbit modeling, which is reported below in mission design section.

Attitude: Spacecraft attitude stability and control are required to within 5°. The attitude stability requirement is derived from the mission requirement for 10% absolute knowledge of the magnetic field. Data collection in shadows and shortly thereafter is not required, but it is highly desirable. Since thermal changes during shadows will affect the magnetometer and particle measurements, as spin rate changes, it is recommended (but not required) that spin rate data be obtained interchangeably from the Sun sensors and the Earth/Moon sensors (infra-red detector).

2.3.2. Spatial Resolution and Number of Spacecraft

DRACO must provide a typical inter-spacecraft spacing (resolution) of ~ 2 Earth radii. Moreover, the distribution of inter-spacecraft spacing should be as narrow as practical, so that random “holes” and “bunches” in the spacecraft distribution are minimized. This requirement is translated into orbital strategy below.

2.3.3. Mission Duration

To achieve its science objectives, DRACO must have a mission lifetime of sufficient duration to observe magnetotail behavior during a variety of solar wind conditions and at least a sampling of typical solar wind disturbances, including corotating interaction regions and CMEs. The entire constellation should be put into orbit with apogees in the local time range around local dawn. Initial activation would then be complete well in advance of the rotation of the tail across the constellation orbit pattern as the Earth orbits the Sun. This would produce a pioneering but ancillary study of the dawn flank of the magnetosphere and its interaction with the magnetosheath, early in the mission. This would be followed by a main mission phase as the constellation passes through the center of the magnetotail over a period of roughly 4 months. This, in turn, would be followed by a study of the dusk flank and boundary layer interactions. All this would occur during the first six months of operation, and would achieve the minimum success criteria for the mission. Continued operations over a subsequent year would produce unprecedented studies of the dayside magnetopause, magnetosheath, bow shock, and foreshock regions in the solar wind. Studies of these regions are of course considered to be ancillary science for DRACO, but would have very high value, and would position DRACO for a second pass through the tail 1-2 yrs after launch.

2.3.4. Data Volume and Flow

The general data flow scenario calls for data from an entire orbit to be stored on board, and then downloaded quickly during perigee passes near the Earth. This will minimize the requirements for transmitter power and ground

operations, but creates the need for on-board storage. **Table** 3 presents the Magnetotail Constellation DRACO science data accumulation rates and total data storage requirements per orbit, absent any data compression. Lossless compression will be used routinely in practice, creating a factor of ≥ 2 contingency in the overall data volumes shown here, reducing the requirement for bulk memory on the spacecraft, and possibly reducing the downlink requirement from that reported here. The typical intrinsic instrument sampling rates will generate the acquisition of a quantity of data from a single spacecraft that is already quite manageable by contemporary standards.

Table 3. Instrument data sampling rates

Instrument	Basis (3 sec spin period)	Data Rate
MAG	16 vectors/spin @ 16bits/sample	768bits/spin
Plasma velocity, ions	8 elevation × 11 azimuth × 16 energy × 8bits/sample	11264bits/spin
Plasma velocity, electrons	8 elevation × 11 azimuth × 16 energy × 8bits/sample	11264bits/spin
Energetic ions	4 elevation × 8 azimuth × 16 energy × 8bits/sample	4096bits/spin
Energetic electrons	4 elevation × 8 azimuth × 16 energy × 8bits/sample	4096bits/spin
Total/Spin		31488bits/spin
Total /120 hrs.	Maximum apogee orbit (40 R_E) data accumulation	3.8 Gbit/orbit maximum

For a constellation mission, modal variations in data taking are undesirable because of the high value placed upon eventual assimilation of identical data from numerous observing points. This assimilation task is simplified by homogeneity of the individual data sets in terms of time, energy, and angular resolution. Thus, the economic advantage of making all the spacecraft and instruments identical is synergistic with the overarching science goals of the mission.

DRACO's lower apogee orbits have reduced storage requirements in accord with the shorter orbital periods, the lowest apogee orbit having a period of ~ 12 hrs. Assuming identical spacecraft, the excess data storage capability in the lower orbits translates into considerable flexibility in the planning of downlinks. All of the lower apogee data can be transmitted during considerably shorter contact periods, or it can be accumulated for multiple orbits and transmitted using the same contact period as the higher apogee orbits. The opportunity also exists for triggered burst mode data collection to be done at higher than normal time resolution, with the burst mode data stored in the contingency memory for the lower apogee orbits. Provision for burst mode collection can also be made for the higher apogee orbits when data compression is implemented.

A summary of a possible scenario including burst data collection is shown in **Table** 4. The lowest apogee orbits can easily collect an amount of burst data per orbit equal to the routine data collection, assuming a data dump can take place once per perigee pass. Lower tracking availability will reduce the burst collection from those orbits. The highest apogee orbits (periods greater than 50 hours, i.e., apogees greater than 20 R_E) must retain most of the memory available for routine data collection. However, they can easily accommodate an amount of burst data similar to that for the lower apogee orbits, simply by forgoing routine collection in the lower altitude parts of the orbit ($r < 7\ R_E$).

Table 4. DRACO Downlink Summary

Spin Period (SP)	3 sec	3 sec
Orbital Period (OP) =	15 hrs min (apogee = 7 Re)	120 hrs max (apogee = 40 R_E)
Routine Accumulation Interval (RAI)	12 hrs min (apogee = 7 R_E)	90 hrs max (apogee > 20 R_E)
Burst Accumulation Interval (BAI)	12 hrs ÷ burst factor	15 hrs ÷ burst factor
Total collection per orbit	128 MByte	640 MByte

2.3.5. Command Uplink

Instrument commanding will be minimal. All commands are time-tagged and uploaded to an on-board buffer in the DPU for delayed implementation. Commands include clock updates, providing information on when to start and stop routine data collection, when to anticipate ground contact next (based on updated contact times), what criteria are to be used to trigger burst mode, and which quantity to burst on. Other options may include changes in the number of burst intervals, software uploads, and on-board processing options, but do not constitute standard commands during routine tracking sessions. In general, instrument mode changes will not be part of the routine commanding unless required for health and safety.

During initial activation, high voltage instruments will be ramped and checked out during perigee pass contact periods, then turned over to automated operation for the rest of their lifetimes. While the first few spacecraft activations may be watched very closely, this operation will become quite routine thereafter.

2.4. Instrumentation Requirements and Strawman Payload Resources

The science requirements can be fulfilled with three principal measurement instruments: 1) Triaxial Magnetometer (MAG) 2) Electrostatic Analyzer (ESA) and 3) Solid State Telescope (SST). The instruments are based on current technology. Anticipated advances in technology can reduce the instruments' size and weight, thereby increasing the number of probes that can be released on a single launch, as well as increased capability for the same weight and power, thus enhancing the science return.

The unique aspects of the science payload for DRACO are:

- The high level of integration of instruments,
- The high level of integration of the spacecraft around the science instruments
- Special design considerations that will render the instrument suite manufacturable in large numbers and capable of rapid testing and calibration as a single unit.

In the following, instrument resource requirements are summarized. These are derived from current technology, with addition of strategy for integration to reduce weight and power down to a minimal amount. The strategy is to implement most of the electronics design on a single board of the spacecraft DPU. **Table** 5 summarizes those resources for three instrument types.

Table 5. Instrument Resource Allocations

Instrument Type	Characteristics	Mass (kg)	Power (W)	Comments
Magnetometer (MAG)	Triaxial Fluxgate,	0.5	0.6	Includes sensor, feedback drive, digital electronics
Electrostatic Analyzer (ESA)	"Top Hat", Dual hemisphere design: Ions and electrons:	2.0	1.3	Includes HVPS and analog electronics
Solid State Telescope (SST)	Twin telescopes back-to-back; (ions and e-'s)	0.5	0.4	Includes HVPS and analog electronics

2.4.1. Magnetometer

Triaxial fluxgate magnetometer capabilities that satisfy science requirements have been demonstrated in previous missions (Lunar prospector, FAST, WIND). Careful design for this mission can also reduce weight and power to make them commensurate with nanosatellites. Ring cores of a few centimeters have been tested in the laboratory and low-weight copper windings have been flown before (POLAR/MFE). A 16 bit digitization is sufficient. Noise levels based on previous flight experience and lab tests are -+0.05 nT. Two ranges are necessary: 1) A low field range (<1000 nT) is necessary for science and is noise-limited, and 2) A high field range (<16000nT), necessary for backup attitude knowledge and ground testing of the unit, is digitization limited (0.05 nT).

The mission will benefit from a Quality Assurance (QA) program that emphasizes the redundancy built into the large number of nanosatellites rather than in a single instrument realization. This makes instrument commanding and mode switching simpler and the instrument lighter. In accordance with this philosophy, a single drive (rather than the traditional triple-redundant) electronics circuitry can be used, which further reduces the power and weight of the instrument.

Early resolution of magnetic cleanliness issues has proven to be commensurate with a low cost, high performance flight unit. All known sources of magnetic material (including the possibility of broom magnets on the SST) must be compensated for early in the program. A clear understanding that there is no expectation for useful data collection during RF operation, must be addressed. A primary consideration for magnetic cleanliness is the current from solar panels which demands careful electrical design and wiring.

Spacecraft shadow operations impart a change in the spin rate due to thermal contraction of the spacecraft body. Shadow data are not mission-critical, but occur in regions where the reconnection or current disruption processes erupt. Salvaging such data should be given careful consideration. One possibility is to use an Earth Infra-Red (IR) sensor to accurately track the spin rate, in addition to the Sun sensor. Automatic switching to the IR sensor once the Sun sensor signal degrades (shadow) will accomplish this goal at little added expense (or at no added expense if the (IR) sensor is already part of the ACS system).

A small (30 cm) boom deployable via centrifugal force shortly after release is expected to be necessary for cleanliness purposes. The weight of the boom (from carbon epoxy based on Lunar Prospector, FAST and POLAR heritage) is 100 grams and has been included in the magnetometer weight given above. An arm boom with a latch would be preferable to a telescopic boom, since it better maintains the MAG mounting orientation after release.

Figure 6 shows the lunar prospector boom latch., and the ROSETTA lander magnetometer. The DRACO sensor can be ~1.5 cm or smaller. Developing technologies will make possible even smaller and lighter magnetometer systems, but this is not essential to DRACO.

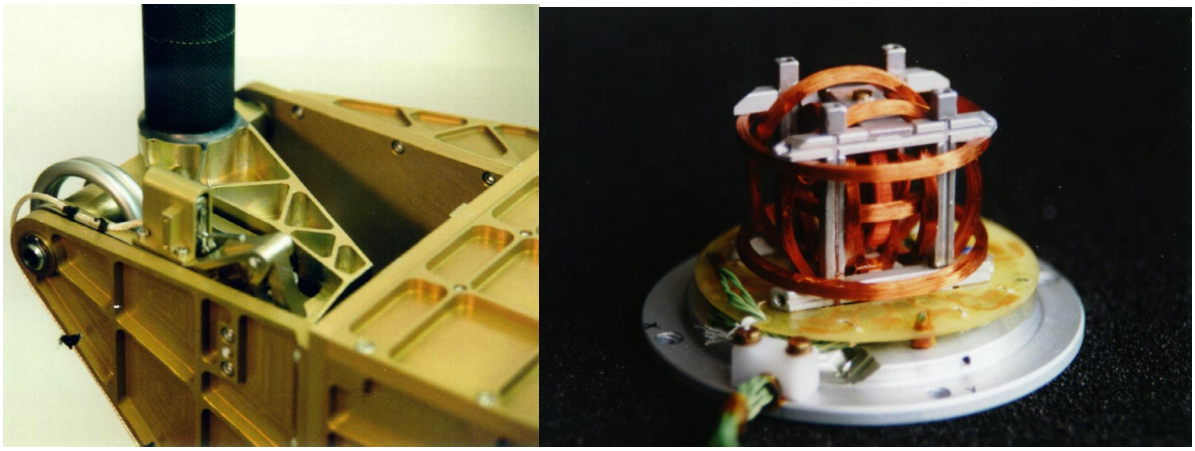

Figure 6. Lunar Prospector magnetometer boom latch (left). ROSETTA lander magnetometer at 50g (right).

On-board calibration is a significant component of the mission success. It is important to ascertain that two spacecraft provide identical values when no currents are present. Existing methods from cross-calibration of CLUSTER magnetometers can be used. These methods call for initial individual calibration of zero levels, gains and sensor orientations, followed by inter-calibration in low current regions of the magnetosphere. The benefits from such a method can surpass any pre-flight ground testing with significant value added to the data. Automating this procedure is essential to limit costs.

2.4.2. Electro-Static Analyzer Plasma Instrument

The ESA instrument measures total ions and electrons at energies between 10 eV and 30 keV. The science requirements of Magnetotail Constellation DRACO can be met with a single analyzer pair (one for ions and one for electrons) on each nanosatellite. These will collect measurements of the complete 3D ion and electron velocity distributions during each spacecraft spin. Particles enter the analyzer over a ~180 degree Field Of View (FOV) and are selected in energy by the potential applied between the outer (0 Volts) and inner (0-3 kV, sweeping) concentric spheres. The particles are focused onto the MicroChannel Plate electron multiplier (MCP). The ~180 degree field of view is aligned with the spin axis so that a full 4π steradian solid angle can be covered each spin. The FAST plasma instrument illustrates the flight heritage of hardware that would be practical to fly on DRACO, while the Medusa plasma instrument for the Swedish Munin spacecraft shows that even smaller instrumentation is being developed currently (Munin total spacecraft mass = 6 kg). Both are based on the dual opposing top-hat concept, as illustrated in *Figure* 7, but the FAST design preserves separate entrance apertures for electrons and ions while in the Munin design the electrons and ions share a common aperture. *Figure* 8 illustrates the assembly of 4 such ESA's for the FAST spacecraft, and the complete Munin spacecraft, weighing only 6 kg, and containing one Medusa ESA.

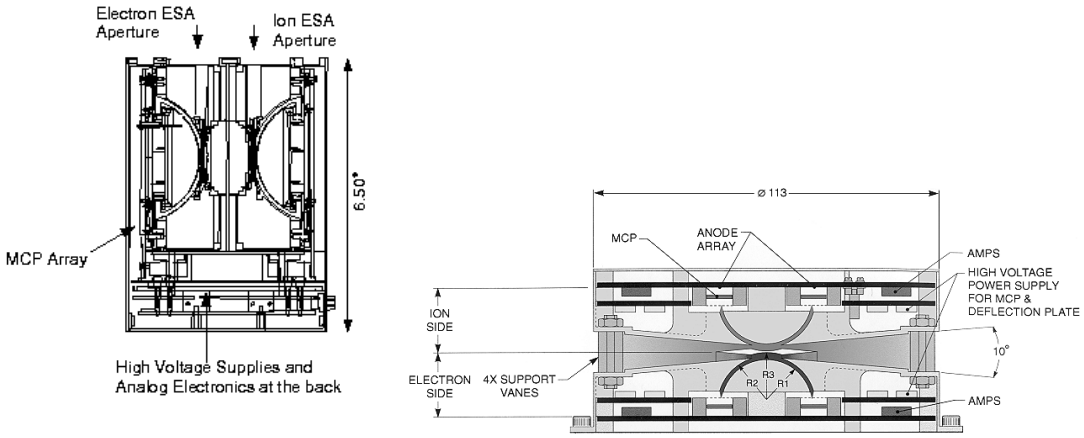

Figure 7. The ESA plasma instrument for the FAST satellite (left panel), and the Munin ESA assembly, known as Medusa (right panel). Both share the dual opposing top-hat concept to observe electrons and ions simultaneously.

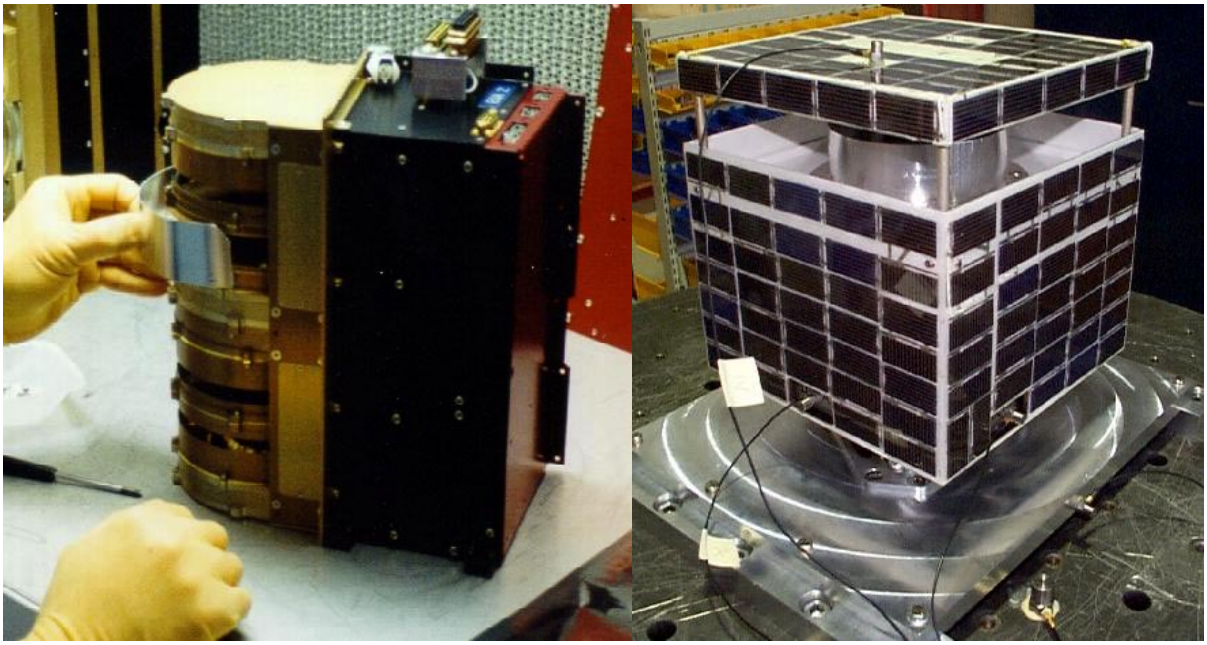

Figure 8. The FAST ESA mechanical structure, including 4 independent fast plasma analyzers (left), and the Munin structure with solar arrays and a single Medusa analyzer, with a total spacecraft mass of 6 kg (right).

Incremental gains in weight and power reduction are expected from development funding using the top-hat instrument principle, or other related optics principles (e.g. the Munin Medusa instrument). However, breakthrough instrument advances may result from the development of delta-doped detectors and other similarly-motivated solid state devices. That principle is expected to reduce the threshold of particle detection in solid-state detectors, which will allow solid state telescopes to operate in the plasma energy range. This is a technology that should be pursued further for DRACO as instrument development funding becomes available.

2.4.3. Solid State Telescope for Energetic Particles

The principle of solid-state telescope detection of total ion measurements has a long heritage in previous missions and can be readily implemented in a way that meets the science requirements of DRACO at a weight and power commensurate with a 10 kg nanosatellite. Using WIND and Equator-S heritage detectors, each double-ended telescope would consist of a set of 3 semi-conductor detectors. The detectors are fully depleted, ion-implanted silicon with very low leakage current. One side detector measures ions, and the other side detector measures electrons. High-energy (400 keV- 1MeV) electrons are measured by the center detector. The operational principle is illustrated in *Figure* 9. Ions are stopped on one side using a Lexan foil and electrons are stopped on the other side using a small "broom" magnet. A pair of such detectors stacked together and using a common magnet yoke is also shown in *Figure* 9 (one pair is shown as deployed on WIND). Analog electronics for pulse shaping amplifier A/D converter and coincidence logic is housed close to the detector, while digital electronics are housed at the spacecraft DPU.

Increased capability can be achieved from new technologies utilizing miniature detector design and Application Specific Integrated Circuit (ASIC) technologies for analog and digital processing. Such capability entails full angular resolution and mass discrimination at no additional weight and power expense. Such technologies currently await flight demonstration in the near future.

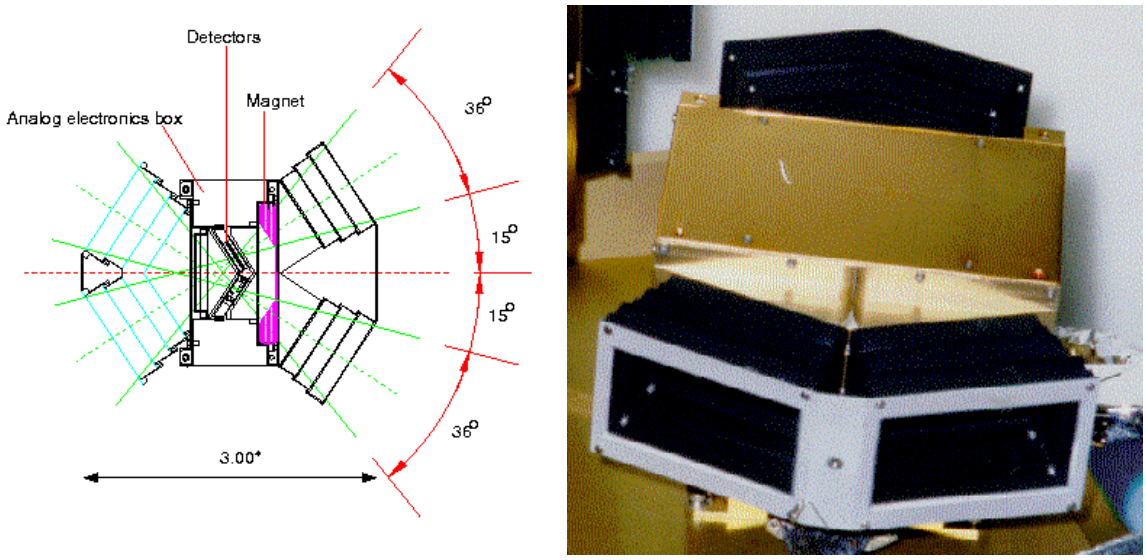

Figure 9. Solid State Telescope (SST) operational concept(left), WIND spacecraft realization of SST (right).

2.4.4. Signal/Noise Requirements

Figure 9 indicates the basis for sensitivity requirements, using data from recent missions (Geotail and WIND). These observations were obtained in the magnetotail from 8 to 30 R_E, spanning variations in flux by an order of magnitude for these representative examples. The pixel geometric factors for successful observations in this region range from 0.0001 cm^2-sr-eV/eV to 0.01 cm^2-sr-eV/eV per pixel for the plasma velocity analyzer, and from 0.01 to 0.1 cm^2-sr-eV/eV for the energetic particles instruments. To assure the required time resolution of 10 sec (~ 3 spins as currently planned) for plasma measurements having an accumulation time at full angular and energy resolution of

0.06 sec (16 energies, 11 azimuths (elevation imaged on 8 anodes), we need ≥ 18 s^{-1} count rate to have meaningful statistics. This is readily attained for the range of GFs used on Geotail and WIND, as seen in the figure.

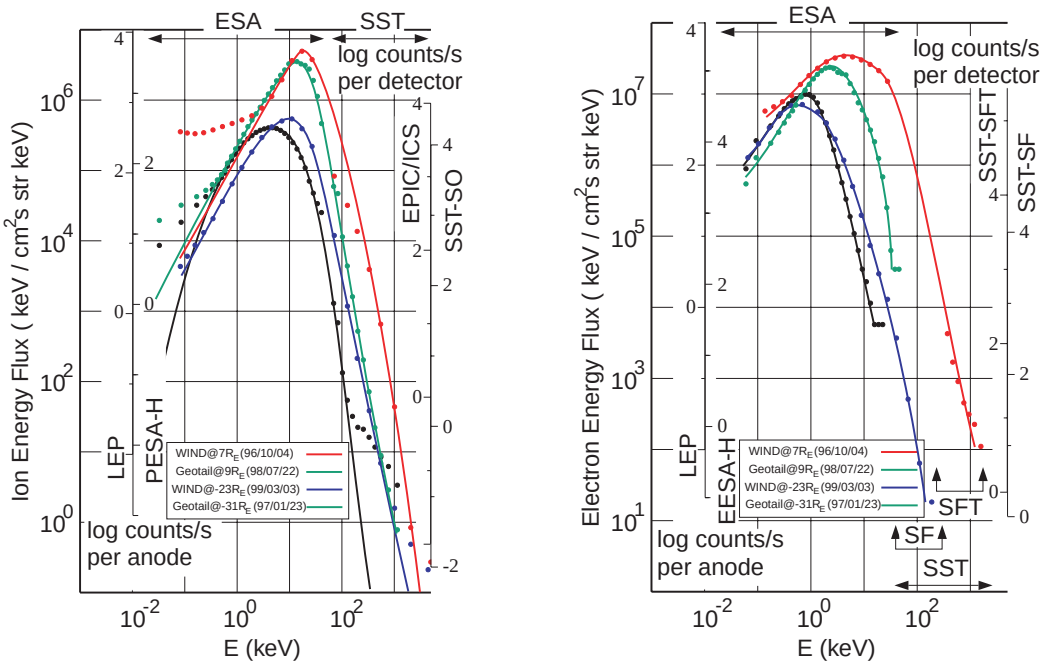

Figure 10. Observations of plasma sheet ions (left panel), and electrons (right panel). Peak fluxes (left side scales) and count rates (inner left and right side scales, also logarithmic) are shown both from the LEP, or low energy plasma instrument, and EPIC/ICS, the energetic particle instrument, on Geotail. Similar results from WIND, closer to the Earth, are derived from the PESA/EESA (plasma instrument), and the SST (energetic particles instrument). Both data points and representative fits are shown. Data courtesy of T. Mukai (LEP), D. Williams (EPIC), and R. P. Lin (PESA/EESA/SST).

To assure the required time resolution for energetic particle measurements having an accumulation time at full angular and energy resolution of 0.08 sec (16 energies, 8 azimuths (elevation imaged on 4 detectors), we need ≥ 13 s^{-1} count rate to have meaningful statistics. This is easily attained for electrons with the range of GFs used on Geotail and WIND, as seen in the figure. For energetic ions, this is satisfied in the range up to a few hundred keV, but some integration will be required for the very high energy ions, with GF's similar to those on Geotail and WIND.

Problematic noise sources for these measurements include UV leaks through the optics, and penetrating MeV electrons. The former can be reduced adequately with careful blackening and baffling. The latter are only a serious problem inside of 10 R_E, but adequate shielding close to the detectors must be included in the instrument designs, since the nanosat structure offers very limited shielding external to the instrument.

Dynamic range is not a serious problem except in the inner magnetosphere, where fluxes increase significantly. Since the DRACO orbits will include substantial periods in this region, adequate dynamic range and/or automated shutdown procedures must be implemented.

3. Mission Design

3.1. Constellation Orbit Strategy

Magnetotail Constellation DRACO must sample the magnetotail region from about 7 R_E to 40 R_E, centered at midnight and extending east and west of the Earth-Sun line by about 10 R_E. The spacing of the spacecraft should be as uniform as possible, given the eventual random phasing of the spacecraft around their orbits. This can clearly be done most straightforwardly using a nested group of orbits with a common perigee and apogees varying over the range indicated above. In this way all of the spacecraft will come through a common region wherein command and data links can be established economically.

The orbits discussed in this section represent the most current thinking concerning the orbit requirements for meeting the Magnetotail Constellation DRACO requirements. The details in the Mission Design sections to follow are based on different orbits and numbers of Nanosatellites than may be presented in this section. Careful study of the constellation orbit options has been performed to determine the number of Nanosatellites that will give adequate spatial coverage.

3.1.1. Trade Study of Orbit Classes

As a basis for quantitatively assessing this strategy, orbit modeling has been performed on a suite of up to 100 virtual spacecraft. In particular, this simulation addresses the spatial separations obtained using various orbital deployment strategies, with an eye toward meeting the mission measurement requirements with the minimum possible number of spacecraft. The principal strategies investigated were based either on families of spacecraft placed evenly around a number of coarsely spaced orbits, or a distribution of single spacecraft in closely-spaced orbits, with random placement of spacecraft in orbital phase. In either case the range of orbital apogees was from 7 to 40 R_E.

Two obvious types of orbits are:

- *Family* orbits, where n Nanosats are equally spaced in each orbit, with N/n different orbits (“strings of pearls”) in the full constellation, where N is the total number of Nanosats. and n varies from orbit to orbit to level the density of spacecraft.
- *Random*, or single orbits, in which N Nanosats are placed in N different apogee orbits, initially spaced uniformly in apogee, but optimally spaced so as to level the density of spacecraft.

Each of these orbit types has advantages and disadvantages. In addition, further study may reveal additional types of orbits, which may or may not be more advantageous. *Figure* 11 illustrates the two current possibilities, by means of 2D plots of the probability density of the spacecraft in 1x1 R_E cells. Without station keeping, currently not a planned capability for the Nanosats, any orbit chosen will be susceptible to perturbations and evolve over time. Thus, it is necessary to pick orbits which will provide the desired coverage over the entire mission lifetime.

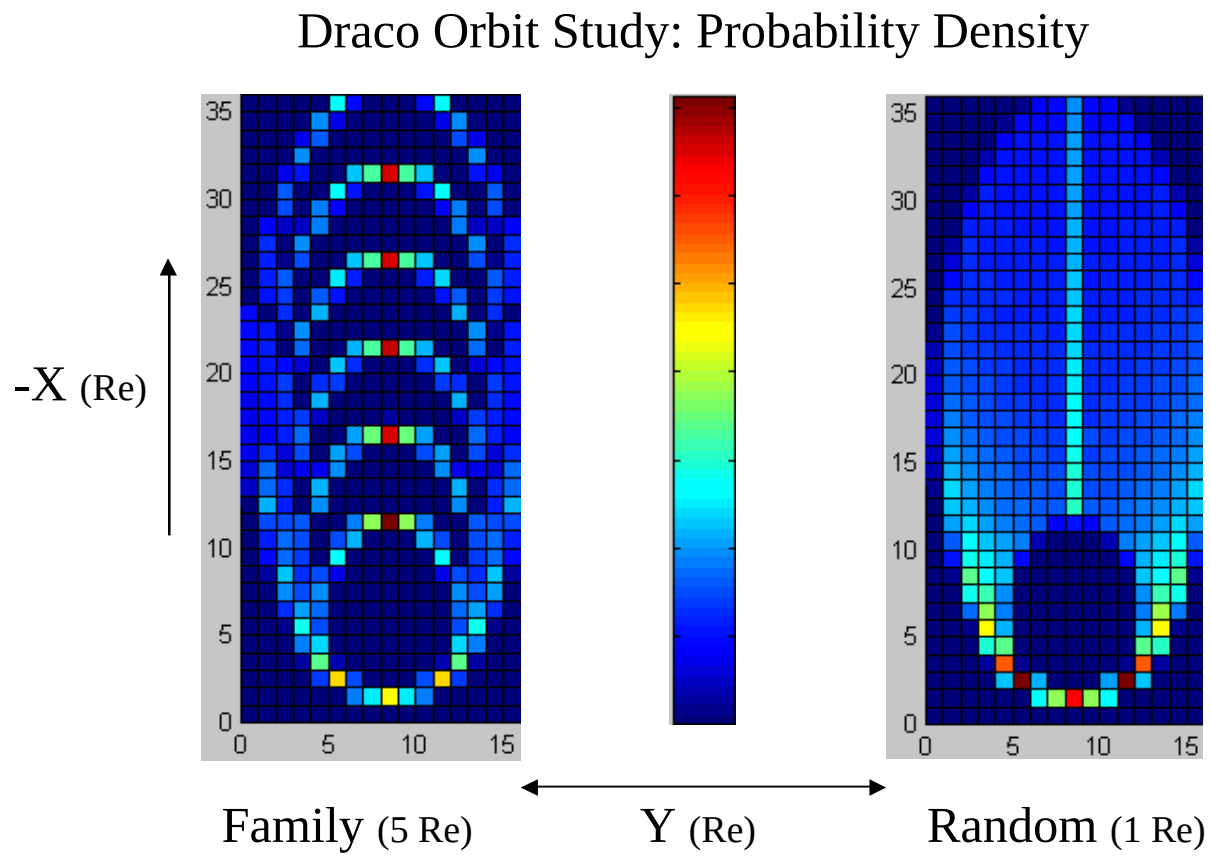

Figure 11. Probability density of 75 spacecraft in family (5 R_E spacing) and single (or random) s/c distributions of orbit apogees, both averaged over random distributions in orbital phase, with all perigees at 3 R_E and apogees extending to 35 R_E. The probability peak at apogee results from slow motion there.

Figure 11 illustrates a snapshot of the orbital configuration shortly after launch, for both the family strategy, and for the random strategy. Examination of numerous such snapshots reveals that the single orbit distribution of spacecraft tends to become reasonably uniform, though some randomly occurring "holes" do occur at times. In contrast, the family distribution remains clumped in radius, leading to undesirable gaps in the distribution, unless the families are placed closer together, which becomes the random distribution in the limit of one spacecraft per orbit.

When the constellations are examined statistically in terms of the distance from each spacecraft to its nearest neighbor, the result is a histogram of nearest neighbor distances, as shown in *Figure* 12. We adopt the most probable nearest neighbor distance as the effective spatial resolution of the constellation. To avoid overly weighting the perigee legs of the orbits, nearest neighbor distances are computed only for the parts of the orbits with X<-10 R_E, here the lowest apogee distance. For 75 spacecraft spread over the range from 10 to 35 R_E, in the either distribution, the resolution is about 1.2 R_E. A requirement for 2.0 R_E resolution allows the number of spacecraft in the constellation to be reduced somewhat. When scaled to a distribution extending from 7 to 40 R_E, the mission science goal is a constellation of 100 s/c. However, the descope floor that barely satisfies the mission requirement for 2 R_E mean spacing, is 60 spacecraft.

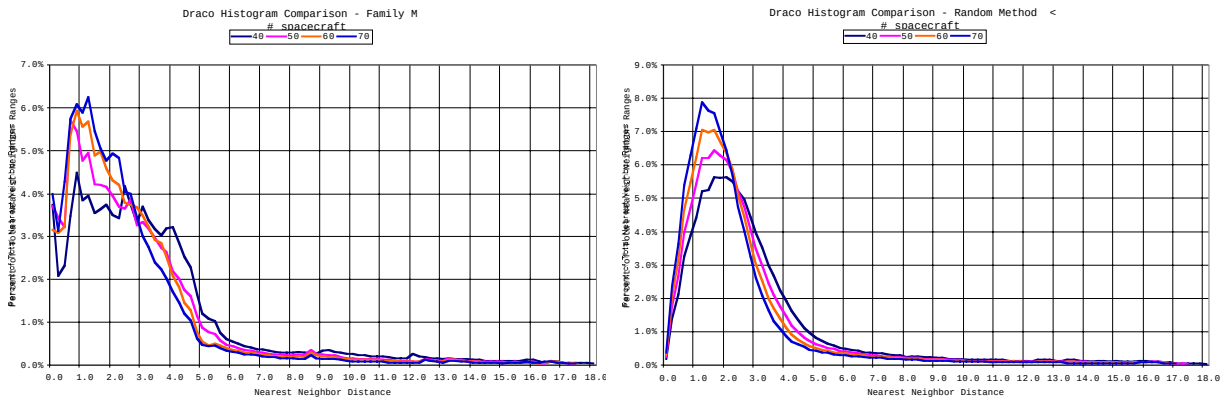

Figure 12. Histograms of nearest neighbor distances for a fleet of varying numbers of spacecraft in both family (left) and single or random (right) distributions of orbital apogees, over the range from 10-35 R_E. The family distribution used here has an orbital spacing of 5 R_E. The region of very high spacecraft densities for X > -10 has been excluded from these histograms.

It can be seen from the figure that the single or random distribution produces the least structured distribution of spacings. As the number of spacecraft decreases, the mean spacing increases, as expected. However, for the family distribution, the change occurs as a shift in the relative importance of along-orbit spacing and cross-orbit spacing, leading to gradual broadening toward 5 R_E, as the spacecraft are spread out increasingly within orbits. In contrast, the single or random distribution remains narrower overall. In this study, the radial spacing of orbits used in the single distribution was uniform. By distributing the apogees appropriately, it will be possible to level the spacecraft probability, as shown in Figure 11, in the radial dimension. This will produce a narrower distribution of spacings, and a more uniform constellation distribution overall, than that shown here.

3.1.2. Constellation Evolution

One of the important considerations about this constellation configuration is how long will it stay together when the orbits evolve. To check this we have calculated orbits using the Merged Simplified General Perturbations Propagator (MSGP4), in Satellite Tool Kit, version 4.03, produced by Analytical Graphics Inc. This software includes moments of the Earth's gravitational field up to the fourth geopotential coefficient, J_4, and includes lunar and solar gravitational effects.

The evolution of the constellation orbits is affected by orbital insertion uncertainties, by lunar and solar perturbations, and by differential precession among the different orbits. Insertion uncertainties will produce some initial spread of the orbits away from the targeted alignments. Lunar/solar perturbations will cause the outer orbits to drift away from the initial orbital plane. *Figure* 13 summarizes and illustrates the manner in which the orbit inclination will evolve over the first two years. Differential precession will spread the inner orbits relative to the outer orbits, splaying the overall constellation out in local time. Figure 14 illustrates and summarizes the orbital precession effects for orbit inclination of 10°(and a slightly different constellation design).

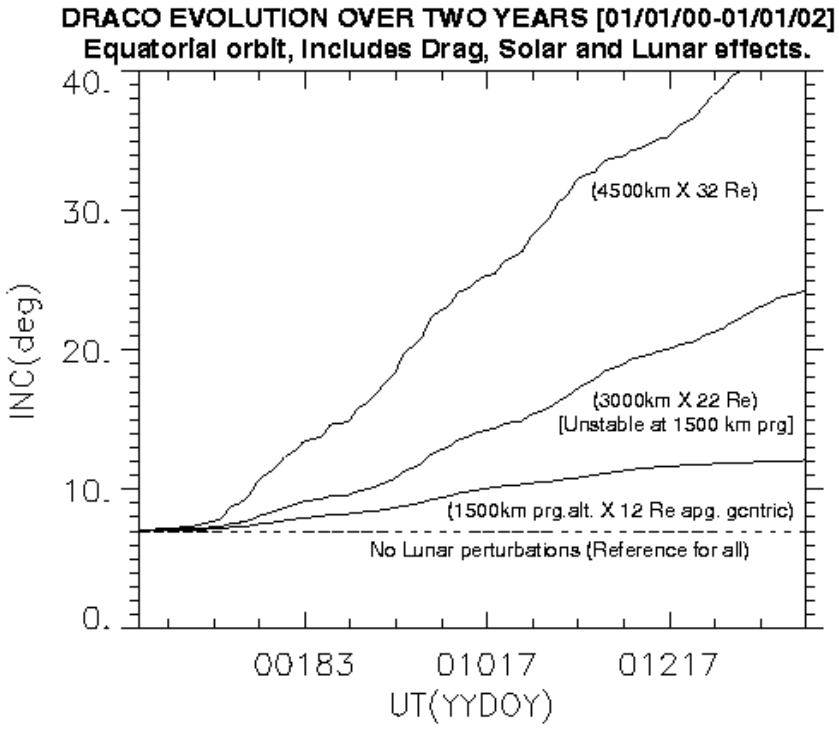

Figure 13. Evolution of typical magnetotail constellation orbits over two years.

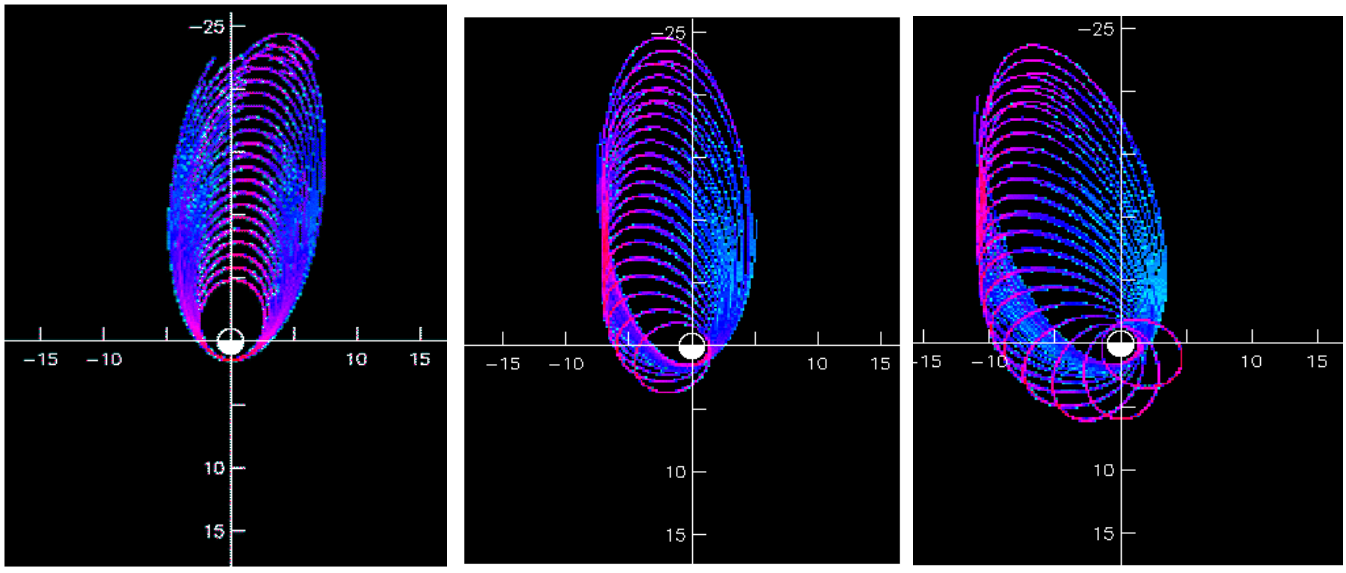

Figure 14. Drift of a constellation of 21 spacecraft over a two year period owing to differential precession of lines of apsides, for orbit inclination of 10°. Spatial frequency of occurrence along each orbit is color-coded in arbitrary units a) at launch, b) after 1 year, and c) after two years.

3.1.3. Deployment Strategy

An appropriate deployment strategy must be employed to maximize coverage and minimize Dispenser Ship complexity and resource requirements. The strategy adopted here supports a single launch of all N Nanosatellites using a unique Dispenser Ship spacecraft that is used to contain and deploy the individual Nanosatellites. The dispenser ship and orbital deployment are discussed in greater detail below. We presently feel that the "Single" approach is preferred over the "Family" - both scientifically and probably for deployment efficiency, as well. If the family approach is used for deployment convenience, the groupings of spacecraft should be kept small enough that orbits are separated by no more than 2 R_E to maintain the required spacing.

3.1.4. Radiation Environment

The expected radiation environment for spacecraft in the DRACO orbits has been evaluated and is a strong driver of the orbital deployment strategy. The choice of $3R_E$ for perigees is largely driven by this consideration, which justifies the marginal increase in propulsion required. *Figure* 15 shows the radiation dose-depth curves for a 12.5 R_E apogee orbit. It can be seen that this environment, while non-negligible, is quite comparable to other mission dose requirements, notably POLAR. On the other hand, DRACO shielding capabilities will be much less than in previous missions, and furthermore, DRACO parts costs must also be kept low. However, the higher apogee orbits will have reduced radiation accumulations, which will alleviate this situation for most of the constellation.

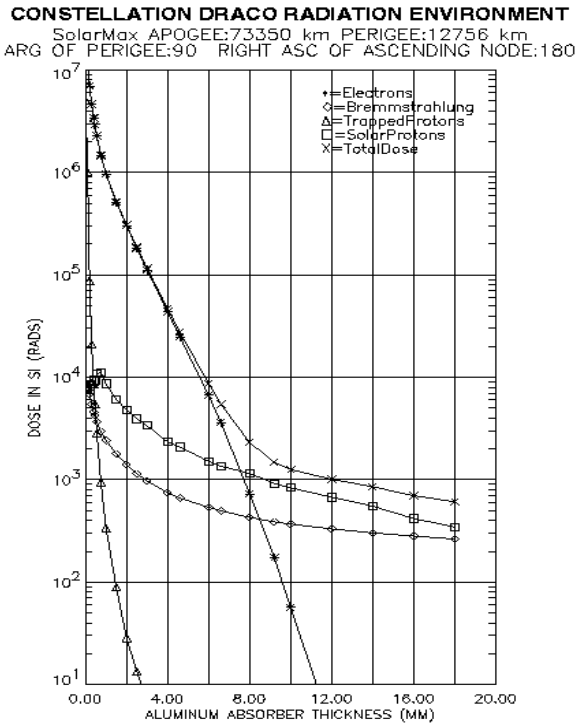

Figure 15. The radiation environment associated with the DRACO orbit shown. Orbital parameters are given in terms of apogee and perigee altitudes, and correspond to 12.5 R_E x 3 R_E geocentric distance.

3.2. Nanosatellites

The information contained in this section is taken from the NASA GSFC Magnetospheric Constellation Mission Document [Lieberman, 1999a]. This document is available from the GSFC STP program office and is posted at the same web site as the present document. The actual mission design and Nanosatellite design will likely change as a result of future studies; the information presented below is strongly dependent upon the assumptions made at the time of the referenced study, including the availability of the enabling technologies previously listed. Many minor changes from the referenced study are included in the material on instruments and orbits given above. In case of discrepancies, the current document (above) takes precedence over the material given below and in the referenced mission document and below.

3.2.1. Requirements And Assumptions

Table 6 provides the detailed set of requirements, which emerged from the Pre–Phase A study completed in April 1999. Subsequent mission technical architecture outlined in this document is derived from these requirements.

Table 6. **Mission Engineering Requirements**

Size	30 cm (12”) diameter x 10 cm (4”) height
Shape	cylindrical disk
Volume	0.007 m^3 = 7,070 cm^3
Number of Probes	Minimum: 44
	Maximum: 104
	Initial satellite spacing within each orbit equal in time
Launch Vehicle	Delta II 7925A
Mission Orbits	All perigees = 3 Earth Radii (Re)
	[Min. case]: 22 highly elliptical orbits (2 satellites per orbit)
	Apogees = 10 to 52 Re in 2 Re increments
	[Max. case]: 26 highly elliptical orbits (4 satellites per orbit)
	Apogees = 10 to 60 Re in 2 Re increments
Mission Lifetime	2 years
Radiation Environment	100 krads total dose over mission lifetime
	Latchup immune
	SEU = TBD
	LET = 90 (TBR)
Deployment	Line of apsides parallel to Sun-Earth line
	Perigee between Sun & Earth
Inclination	Typically 7.5° from Earth equator initially
	Initial Minimum: 0° from Earth equator
	Initial Maximum: 15° from Earth equator
	Inclination angle expected to change as much as 40° due to lunar and other perturbations over the life of mission.

Table 6. Mission Engineering Requirements (cont.)

Orbit Periods	0.97 days for Ra = 10 Re 10.4 days for Ra = 60 Re
Orbit Position Control	+/- 0.5 Re at each apogee (0.833% of apogee radius)
Orbit Position Knowledge	Science requirement: ±20 Km
	Communications requirement: ± 60 Km
Eclipse Duration	Less than 1 hour (greater if orbit plane is in ecliptic)
	Duration maximizes twice a year near orbit equinox
Instruments	Electron detector
	Ion (proton) detector
	Magnetometer
Mass	10 kg (includes orbit insertion and attitude control fuel)
Power	4.5 watts continuous, generated by body mounted solar cells; batteries for eclipse and downlink periods
Battery	1000 cycle lifetime: 7 amp-hrs at 3.3 volts
	30% max depth of discharge
	700 cycle lifetime: 2 amp-hrs at 3.3 volts
	50% max depth of discharge
Power Bus Voltage	3.3 V +/- 5% regulated
Thermal	[passive] insulation and coatings only
	[active] mini capillary pumped loop (mini-CPL)
Stabilization	Initial spin = 40 to 60 RPM from launch vehicle
	Final spacecraft spin >= 20 RPM with axis normal to ecliptic
Attitude Control	spin stabilized by cold gas micro-thruster
	20 rpm = 1/3 rev/sec
	Spin rate knowledge: $< 2x10^{-5}$ rad/sec
	Spin axis position knowledge: < 0.1°
	Spin axis drift rate: < 0.1° over 30 days
Orbital Maneuvers	[10 Re apogee] deltaV = 3000 N-s
	[60 Re apogee] deltaV = 7000 N-s
Sun Synchronization	Sun sensor
	Step rate = 2000 Hz (TBR)
	Resolution = 0.1°
Inertia	Izz/Ixx > 1.05
Instruments Data Rate	1.6 Kbps total for all instruments
Overhead Data Rate	400 bits/sec for encoding, housekeeping
Recorder Data Rate	2 Kbps
Data Storage	SSR (memory stack in multi-chip module)
	Maximum: 1792 Mbits for 60 Re apogee orbit (249 hours storage)
Transmission Rate	Up to 100 Kbps
Command Rate	1 Kbps

The Magnetotail Constellation Mission is enabled by advanced technology. It is constrained in terms of the number of spacecraft within the constellation by the size and mass of the Dispenser Ship and each Nanosat. The capability of the Delta II launch vehicle to place the Dispenser Ship and the Nanosats into orbit is also a key factor. In order to populate the Magnetotail Constellation with the greatest number of Nanosats and still fit within the fairing of the 7925-9.5 Delta launch vehicle, a total of approximately 100 Nanosats were sized for the mission. The mass of each Nanosat is 10 kg as shown above. In order to meet the size and weight constraints of the Nanosats, advanced technology must be employed. The following sections describe the Nanosat subsystems and related technologies.

3.2.2. Mechanical Subsystem

The Mechanical Subsystem (**Table** 7)is comprised of a Structural Bus, a release mechanism for deployment from the Dispenser Ship, and the deployable Instrument Boom.

The structure physically supports all components through launch and operational scenarios. It is an octagonal prism 30cm across the flats and 10cm high. The Bottom Deck is composite honeycomb; the side-walls which support body-mounted solar arrays are made of a thermally isolated, filament-wound composite shell. The Top Deck has high thermal conductance, and is made of either honeycomb or ribbed face-sheet. The precession thruster, ultra-stable oscillator and one instrument detector are mounted on the Bottom Deck. The remaining boxes (including command and data handling (C&DH), instrument, and battery) are mounted on the Top Deck for improved heat dissipation. The communication antenna is mounted to the Top Deck and is aligned with the spin axis.

The release mechanism resides almost entirely on the DS. It consists of a set of prongs protruding from arms sticking out from the DS. The prongs fit into fittings embedded in the spacecraft vertices. Thus the spacecraft is clamped in place during launch. One set of prongs can pivot about an axis parallel to the spacecraft spin axis, allowing a simultaneous deployment and spin-up of the spacecraft. The Magnetometer is deployed on a boom in the radial plane of the spacecraft CG. The structure is designed to a 1.5 Factor of safety on ultimate. Radiation shielding is used only on the 3 most sensitive components: C&DH, communications and Power Supply Electronics (PSE).

Table 7. Nanosat Mechanical Requirements

Item	**Requirement**
Overall spacecraft structure (not including antenna, thrusters, and instrument protrusions)	10cm high by 30cm diameter; magnetically “clean;” minimize sharp corners; passively spin-stabilized
Weight	2.5 kg
Operating Temperature	-80 to +50 °C
Nanosat spin axis attitude during deployment	Spin axis aligned to perigee velocity vector to 1 deg (0.5 deg from ds + 0.5 deg from Nanosat)
Nanosat spin axis attitude during free flight	Spin axis perpendicular to ecliptic to within +/-.5 deg;0.1 deg cone angle
Science mode spin rate	20 rpm
Launch loads	10G in X, Y, Z; GEVS qualification-level random
Frequency	60 Hz axial; 30 Hz lateral
Acoustic	Delta II levels

The structure for the Magnetotail Constellation DRACO Nanosatellite will be graphite composite, cast aluminum, injection-molded composite or a combination of these. Components will be attached to the upper and lower decks through inserts bonded in the material. Thermal conduction is assured through physical contact with the surfaces.

Advanced structure technologies under consideration include:

- Power system integrated into the structure (*Figure* 16).
- Thermal system integrated as part of the structure [micro-machined (MEMS) louvers - *Figure* 17]
- Harness interconnections within the structure
- ACS in a structure (structurally imbedded propellant lines, valve and nozzle)

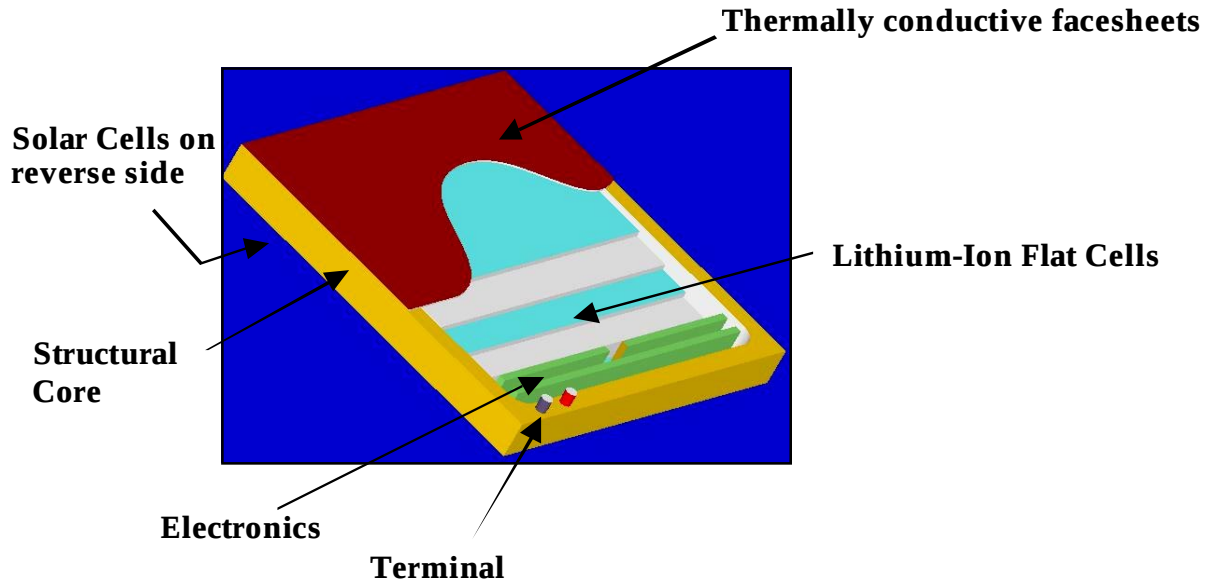

Figure 16. Power System included within a structure.

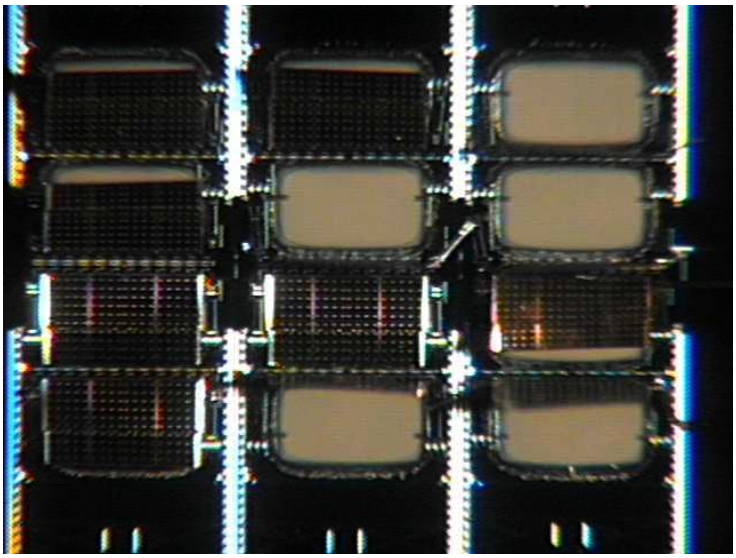

Figure 17. Thermal Control within a structure (MEMS louvers)

3.2.3. Command & Data Handling

Table 8 summarizes the requirements specific to the Command and Data Handling subsystem.

Table 8. Requirements for the Command and Data Handling (C&DH) subsystem.

Item	Requirement
Power	0.8 Watts
Weight	0.25 kgrams
Radiation	100k Rad Si (Total Dose)
Data Rate From Instrument	10 kbit/sec
Data Storage	4 Gbits
Uplink/Downlink Protocol	CCSDS
Uplink Rate	1k bits/s
Downlink Rate	640 kbits/s

To meet the power requirements a combined effort in the reduction of mass, power, size, and cost is underway to produce optimal electronics. The CMOS Ultra Low Power Radiation Tolerant (CULPRiT) system on a chip and "C&DH in your Palm" are technologies that will enable the power reduction required for nano-satellites. The goals of these technologies are a 20:1 power reduction over current 5 volt technology, foundry independence of die production, and radiation tolerance. The Nanosat C&DH architecture will incorporate CULPRiT devices in a multi chip module (MCM) Cube. A non-functional model is shown in *Figure* 18 below.

Figure 18. Multi-Chip Module C&DH

The C&DH subsystem is made up of 6 functional slices of the cubic stack. The processor slice will process commands, make data packets, perform the timekeeping functions, perform ACS computations and control power. The instrument slice will interface to the instruments via an I^2C bus. This slice will also manipulate the data into the required format. The memory slice (or slices) will contain 2 Gbits of SRAM or DRAM. The ACS Interface slice will interface to the Earth/Sun Sensor (Analog data), attitude thruster (pulse command) and orbit thruster (single pulse). The housekeeping Interface slice interfaces to the PSE and reads other analog telemetry such as thermistors,

voltage and current monitors. The last slice is the uplink/downlink card, which interfaces to the transmitter and receiver. This card sends CCSDS packet telemetry to the ground and receives CCSDS packet commands and processes them. The nanosat architecture is shown in *Figure* 19.

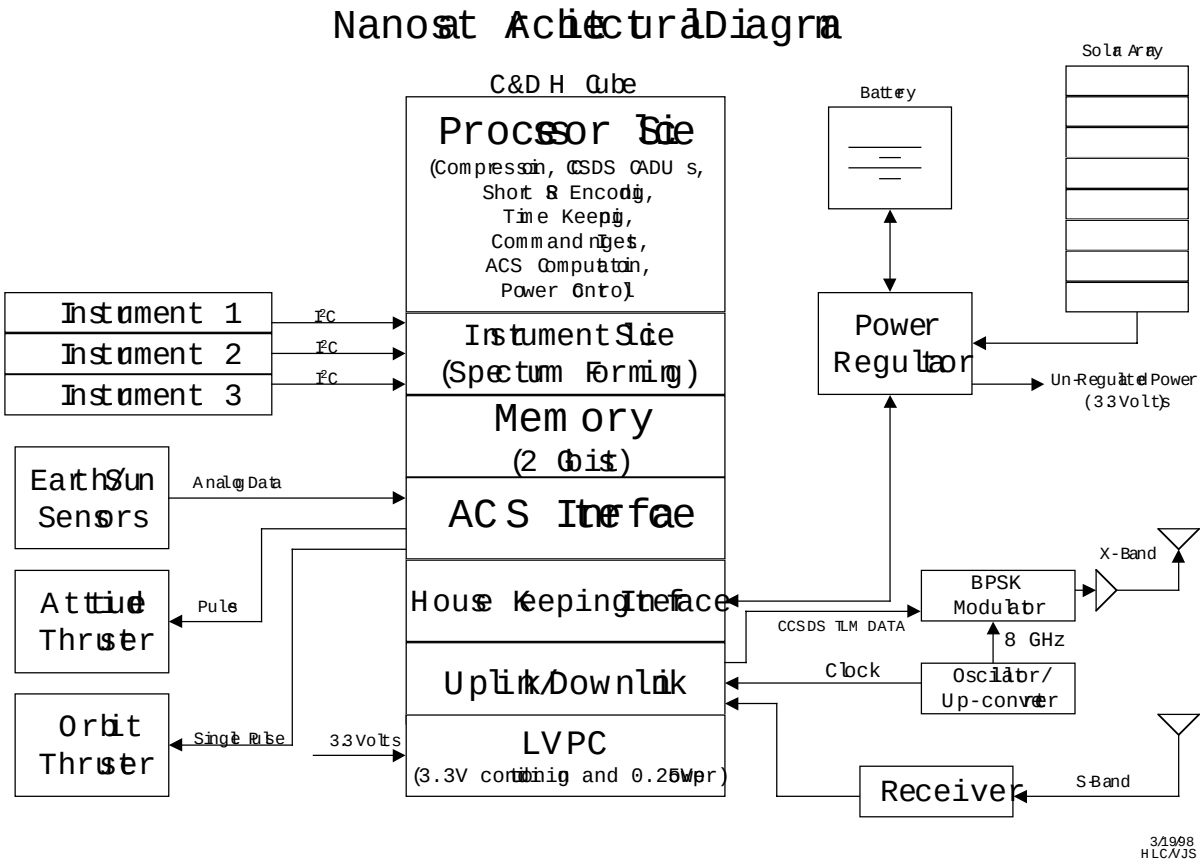

Figure 19. Block functional diagram of the nanosat architecture.

3.2.4. Flight Software

Software embedded in the flight computer/s will perform control functions for the spacecraft. The software function can be resident in a centralized computer or be highly distributed. The software will enable as much onboard Nanosat autonomy as is feasible. With a constellation of as many Nanosats as is needed for the Magnetotail Constellation DRACO mission and the limited ground station coverage/capability (for technical & cost reasons) an autonomy function is desirable. The objective of the Nanosat autonomy effort is two fold:

1. Maximize the scientific return given the limited telemetry resources.
2. Minimize the need for ground-based control of the constellation.

The flight software will have to be very capable to handle routine spacecraft bus and instrument operations. It will also have to be sophisticated so as to handle contingency mode operations upon detection of anomalous operation in any of the spacecraft subsystems or instruments. As a goal, it is envisioned that many, if not most, of the software

functions previously performed for spacecraft on the ground will be performed on-board the spacecraft. **Table** 12 provides some examples of the Nanosat flight software functional capability.

Table 9. Nanosat Flight Software Functional Capability

Subsystem/Function	**Examples**
Operational Mode	Operate, Safe spacecraft
Mechanical	Deployment
C & DH	Telemetry, commanding
Instruments	Operations and data processing
Thermal	Louver/heater control
Power	Regulation; charge /discharge
RF Communications	Ground station data dumps
Propulsion	Time of firing
Attitude Determination and Control	Sensor processing; control software; reorientation maneuver calculation

3.2.5. Attitude Control and Orbit Determination

The Nanosats will have the capability to perform attitude control and orbit determination throughout the mission. The DS will perform initial orbit determination but aside from placing each Nanosat in an initial elliptical orbit there will be no further orbital control.

The requirements for each Nanosatellite are based on the simple spin stabilization chosen as baseline. Miniature Sun and Earth sensors will be employed on each spacecraft. The miniature precision “fan” type Sun sensor will locate the Sun on the celestial sphere during every spacecraft rotation. The following table denotes the mission orbit requirements for initial orbital positioning upon separation of the spacecraft from the DS; these requirements are not used for station keeping of the spacecraft.

Table 10. Nanosat Orbit Requirements

Orbit	**Requirement**
Control	+/- 0.5 Re @ each apogee
Knowledge	
Science	+/- 20 km
Communications	+/- 60 km

Four orbit determination concepts have been identified, which are considered appropriate for the mission.

- Magnetometer methodology
- TDRSS Onboard Navigation System
- Global Positioning System
- Ground Based Orbit Determination System

More detail on each of these methods can be found in the full report [Lieberman, 1999a].

3.2.6. Propulsion Subsystem

There are two technology development approaches being considered for the propulsion subsystem. One is a low power, miniature, cold gas thruster approach (attitude control only) and the other is a low power, hydrazine mono-propellant thruster approach. The latter approach has the potential to satisfy both delta-V and ACS requirements. These two approaches are discussed below.

The low power miniature cold gas thruster approach takes the form of a simple blow-down cold gas system for re – orientation maneuvers. Existing valve technology will not meet requirements. Technology drivers associated with this approach are low power/voltage coupled with high inlet pressures and response times. In addition there are leakage and cost issues which will be addressed in future development/studies. **Table** 11 provides the technology goals associated with this concept.

Table 11. Nanosat Cold Gas Thruster Performance Goals

Item	**Goal**
Power	< 1 W
Voltage	3.3 +/- 0.4 V
Minimum I - bit	44 mN-sec
Pressure Range	100 - 1000 psi
Response Time	5 msec
Leakage Internal External	 < 1x10–4 sccs He (1x10-5 goal) <1x10-6 sccs He
Pulse Frequency	>/= 1 Hz
Cycle Life	1000
Flight Mass	50 g
Isp	60 sec

The low power mono-propellant Hydrazine thruster alternative to the cold gas thruster features a unique valve approach. The technology driver is the low power approach coupled with the required response time. **Table** 12 below provides the goals associated with this alternative approach.

Table 12. Nanosat Mono-Propellant Hydrazine Thruster Performance Goals

Item	**Goal**
Average Vacuum Thrust	0.445 N at 250 psi
Minimum I - bit	44 mN - sec
Inlet pressure	100 - 400 psi
Power	1 W max
Voltage	3.3 +/- 0.4 V
Duty Cycles	0.100 sec on/30 sec off (0.3%) 0.100 sec on/3 sec off (3%) 60 sec on (steady state)
Response Time	30 msec to 90% thrust
Isp	220 sec

Other Possible Nanosat Technologies: Aside from the technologies baselined above, other approaches are being investigated:

- Solid propellant Micro Electro Mechanical System (MEMS) based thrusters. This work is being undertaken at the NASA/Glenn Research Center. It is applicable to attitude control type maneuvers.
- Advanced Mono-propellants. This would entail a potential partnership with the NASA/ Glenn Research Center and a commercial vender. It is applicable to Delta-V and ACS type maneuvers.
- Solid Gas Generator for cold gas thrusters. This has applicability to ACS applications

3.2.7. Power Subsystem

The electrical power system will be comprised of Triple Junction (TJ) GaAs solar cell on eight (8) flat panels of dimensions 11.5 cm x 10 cm each for converting solar power to electrical power and Lithium Ion (LiIon) batteries for energy storage. The Electrical Power System (EPS) delivers an average power of 4.0 watts to the spacecraft and instrument loads. Beginning Of Life (BOL) maximum power available from the solar array is 7.0 watts with an End Of Life (EOL) at 5.71 watts at the end of a 3 years. The energy storage is two 1.2 ah LiIon batteries sized to handle the peak power of 4.39 watts or a option of handling a survival power of .711 watts for a 1.17 hour eclipse at a 60% Depth Of Discharge (DOD). The driver for the solar array size is the condition where average power of 4.0 watts is supplied to the bus while the batteries are being charged from a 1.17 hour eclipse. Batteries can be used to augment the solar array during non-eclipse periods when the transmitter is operating. A margin of 25% is included in the load analysis.

Additional detail is available in the full report, including discussion of other technologies offering future potential.

3.2.8. RF Communication Subsystem

The laws of nature place limits on how far we can push a given technology. The solar energy density and the size of the panels on the spacecraft limit the electric power available to a spacecraft. Solar cell efficiency can be increased from 20 % to 40 %, a factor of 2 improvement, but not by an order of magnitude to 200 %. For this, a new technology is required. The noise background and the transmitted energy per bit (Eb) limit Radio Frequency (RF) communication data quality. Once we get close to the physical limitations, we must change the technology to get more than an incremental improvement. The table below shows the expected requirements for a Nanosat X-band transponder.

Table 13. Nanosat X-band Transponder Specifications

Frequency	**X-band**
Operating Power	3W (12-24V)
Receiver Data Rate	Up to 4Kbps
Transponder Date Rate	> 1 Mbps
Transponder Mass	0.15 Kg (5-10 Kg)

Numbers in parentheses are typical for current state-of-the-art

Communication Requirements

- Transmit science data to ground
- Receive commands from ground
- Generate signals required for orbit determination

Communication Derived Requirements

- Transmit science data to ground
- Use communications coding to reduce power required for transmission
- Power density at Earth shall be at least $1.3x10^{-17}w/m^2$ = -168.9 dBw/m^2 so that ground antenna need not be larger than 11m.
- Power density shall be less than …w/m^2/4KHz to be below RF flux density limitations.
- Data rate of approximately 256 Kbps so that communication time is not unreasonable.
- Receive commands from ground.
- Sufficient solar array capacity for receiver constantly on.
- C & DH ability to decode and act on commands.
- Generate signals required for orbit determination.
- Oscillator frequency stability when in sun light $< 5 \times 10^{-8}$/day so that one way doppler can be used for orbit determination.

Additional discussion can be found in the full report, including communications link budgets.

3.2.9. Thermal Subsystem

The Nanosat preliminary thermal design is primarily a passive design consisting of MultiLayer Insulating blankets (MLI) and selected surface-finish applications. The MLI will be used to reduce losses to and gains from the environment. This preliminary passive design philosophy incorporates a low cost approach to maintaining temperature requirements throughout the Nanosat payload.

Additional details and other approaches are discussed in the full report. The results of this study, to date, help to indicate a direction the thermal design should take as details evolve. The thermal design presented here is a first-cut in the Nanosat feasibility study. It may not reflect the actual configuration of the Nanosat but is based on thermal design guidelines available at the time. The model will later be refined to support any systems design tradeoff studies and detailed design as required.

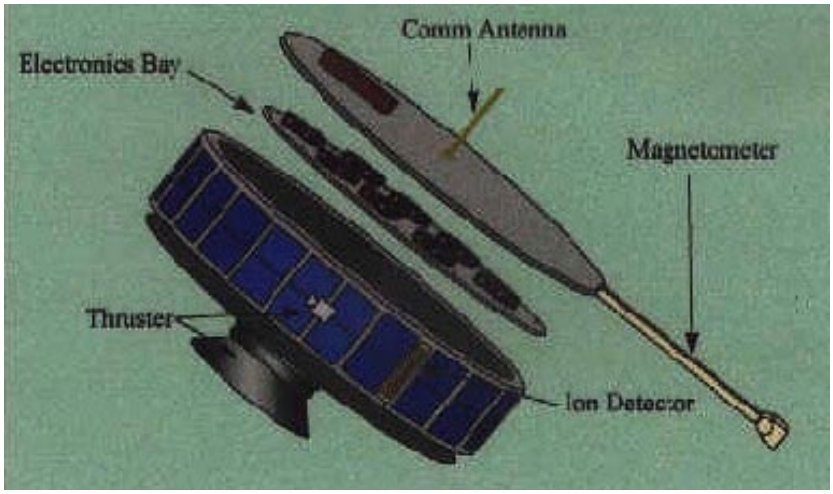

Figure 20. Conceptual view of the nanosatellite for Magnetotail Constellation.

3.3. Dispenser Ship

The details presented herein for the Magnetotail Constellation DS are given by Lieberman [1999b]. That report also references and draws upon the Magnetospheric Constellation Mission Document [Lieberman, 1999a]. The actual mission design and dispenser ship design have changed and may change further as a result of future studies. The information presented below is strongly dependent upon the assumptions made at the time of the study, especially the Nanosatellite configuration described in Section 3.2. As previously pointed out, the orbits upon which the following details are based are not necessarily the orbits presented in Section 3.1. In case of discrepancies, the information given in earlier sections takes precedence over the materials in this section.

3.3.1. Orbital Maneuvers of the Dispenser Ship

Six methods for placing the Nanosats in orbit were studied. The final orbit selected was the least complicated and minimized the Nanosat propellant mass requirements.

For the orbit selected, the Delta places the DS in an elliptical orbit whose parameters are perigee 185 Km, apogee 20 R_E with inclination of 28.7°. The DS performs an apogee burn and raises the perigee to 1000 Km and makes a small change in the inclination. A second apogee burn raises the perigee to 3 R_E and removes 21.2° of inclination. The parking orbit of the DS is 3 R_E perigee, 20 R_E apogee, 7.5° inclination with the line of apses lies in the ecliptic. From the parking orbit the several Nanosats are released with their spin axes aligned to the DS perigee velocity vector. The Nanosat kick motors are ignited at perigee. Some Nanosats will raise their apogees and others will fire in retrograde direction to lower their perigees.

Although the details presented in this report are based on delta-V capability for the Nanosats, it has not been determined at this stage of formulation if this capability will be the final Nanosat requirement. Another option under consideration is to design the DS with the capability to ensure proper Nanosat orbit insertion. However, details of this option are at a very early stage of maturity. Having the Nanosat orbits determined solely by how and when they are released from the mother ship could have significant impact on the requirements and design for a release mechanism; this has not been looked at. Again, it is to be noted that the details to follow are based on the nanosats having delta-V capability.

3.3.2. Nanosat Orbital Maneuvers and Mission Operations

Four Nanosat release mechanisms have been proposed. The kinematics of release have been simulated and it was found that all four will provide for a non-interference separation of the Nanosat from the DS. They all have a common operational interface i.e. the requirement for a discrete electrical command which will cause the force holding the Nanosat to the DS to cease to exist in a short period of time, approximately 1 msec. The command will be given simultaneously to up to 14 Nanosats. When released the rotating Nanosat will “fly” tangentially away from the DS. The angular rate will be approximately the same as that of the DS. The command receivers of the separated units will be turned on, however, only one will have its transmitter on. After the Nanosat’s kick motor has fired (the one with the active transmitter), the ground station, using the nominal burn trajectory for a reference orbit, will point its antenna at the Nanosat. The Doppler shift of the transmitted signal will be used to determine the Nanosat orbital velocity and by analysis the ground station will be able to determine the Nanosat’s orbit.

When the Nanosats are dispensed, they will be selected such that no two satellites will be transferred into an orbit with same apogee. This requirement will assure 1) the ground station has adequate time to track the Nanosats and 2) the true anomaly of satellites in the same orbit will be different. If 10 Nanosats are dispensed at 2 R_E separation no more than 4 will be in an orbit whose apogee is less than 20 R_E. Thus the ground station will be able to get the 30 minutes of tracking per Nanosat needed to get "good" data for each of the 4 "lower" apogee Nanosats before they leave the search field. The ground station can then turn it attention to the remaining 6 Nanosats destined for the higher apogees. Approximately 200 (325-120) minutes (33 minutes per satellite) are available to track the remaining 6.

3.3.3. Dispenser Ship Overview

The heart of the system is the Command and Data Handling (C&DH) system. The X band receiver, located in the Communications Subsystem receives the ground commands. They are decoded and stored in the C&DH as relative or absolute time commands. The ACS sensors send attitude signals to the C&DH, where they are processed to determine the actuator commands (5 thrusters) that are needed to maintain attitude control or to maneuver the DS to a new attitude. The C&DH issues release commands to the Nanosats via the arm and fire relays. The C&DH also send commands to the main thruster during each of the two orbit change maneuvers. Finally, the C&DH processes and formats, housekeeping, status, and health and safety telemetry for transmission to the ground. The dispenser ship architecture is shown in *Figure* 21.

Each subsystem is briefly described in the paragraphs that follow; a more detailed discussion of the dispenser ship can be found in the full report referenced above.

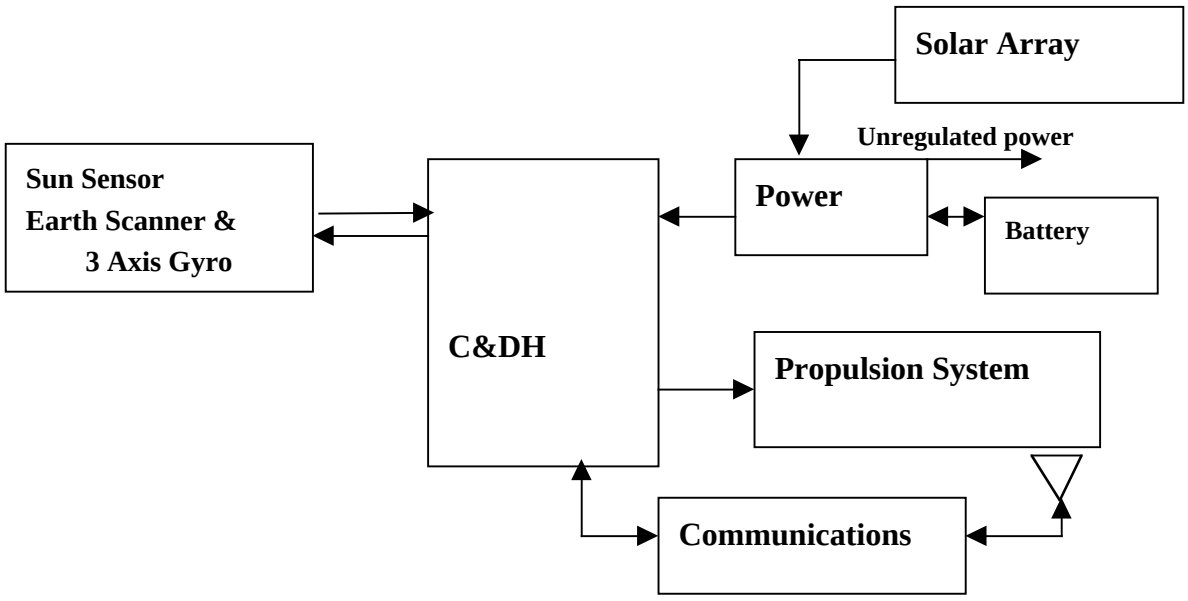

Figure 21. Dispenser ship architecture.

Mass and Power Summary

Table 14 summarizes the final, "as-designed" mass and power of the DS concept presented herein. A more detailed breakdown of mass and power for each subsystem is presented in the following paragraphs.

Table 14. Final as Designed Mass and Power

Subsystem	Mass Kg	Power Watts
ACS	7.1	13.8
C&DH	12	2
Communications	7.8	7.2
Power	5.6	32
Propulsion	50	-
Harness	4.5	0
Thermal	4.5	5
Structure	131	0
Total As Designed	216.9	60

Mechanical Configuration

Figure 22 shows the mechanical configuration of the Nanosat DS. The blue ring at the top is the 130 watt solar array. Above the array is the X band omni antenna. Located on the top ring are 3 coarse Sun sensors, Earth sensors and a fine Sun sensor.

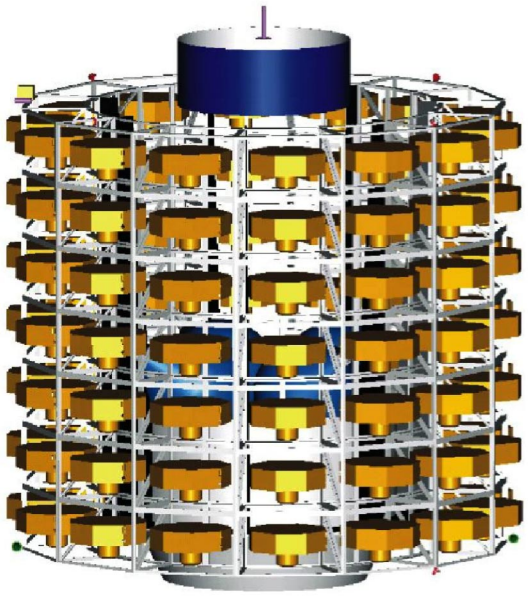

Figure 22. Conceptual mechanical configuration for nanosatellite deployer ship.

In this version, 92 Nanosats are located in individual bays. There are 14 bays per tier and 7 tiers, a total of 98 bays. Since the lift mass of the Delta only permits a payload of 92 Nanosats 6 bays will be empty. Located in area around the base of the DS are, the main thruster, 3 more coarse Sun senors an 4 small thrusters. The propulsion tanks, power

regulators and the avionics are housed in the interior of the DS. The following sections will give the details of the structure, dimensions of the DS, location of the components, mass of the structure and a description of the bay construction.

BOL inertia ratio (MOI around a principle axis to the MOI around the spin axis) is 1.17. The EOL inertia ratio is 1.07. Because of this favorable inertia ratio maintaining the spin about the thrust axis of the main thruster will not require active control.

ACS Subsystem Description

The ACS block diagram is shown in *Figure* 23. The Earth sensor and fine sun sensor are used for attitude references and to measure the spin rate. The ring laser gyro is used as attitude reference to precess the spin axis to a desired attitude and for sensing and controlling the nutation of the DS. The normal mission attitude of the spin axis is perpendicular to the ecliptic except during the portion of the orbit when the Nanosats are to be released. Prior to release the DS will be commanded to precess the spin axis to be parallel to the velocity vector at perigee. Close to the perigee (exact time is TBD) the Nanosats will be release and the scenario describe in section 3 will commence. Precession will be accomplished by the actuation of the bi-propellent thrusters.

Six coarse sun sensors have been provided. From their outputs the position of the Sun with respect to the DSwill always be known, excluding the time when the Sun is occulted. This information from the coarse sun sensor will be use during the initial stabilization phase after the DS has been released from the launch vehicle. To precess the spin axis of the DS from the release attitude to the normal operational attitude (perpendicular to the ecliptic), the attitude the thrusters are used.

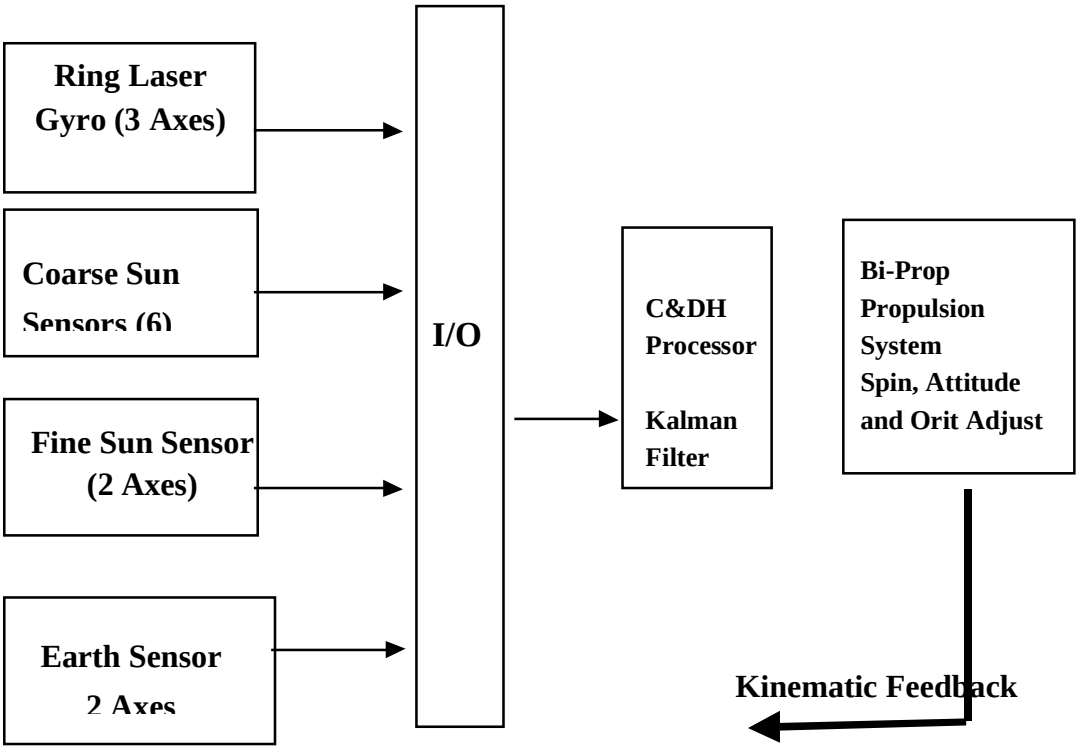

Figure 23. Block diagram of the Dispenser Ship attitude sensing and control system.

Care will be exercised to assure that the FOV of the sensors are not occulted and that uncertainties in the sensor outputs will not be caused by reflections from near by bodies on the DS. To the first order, in the mechanical design, the impingement of the thruster plume on the DS has been avoided. Due to mass constraints and geometrical factors, there are 98 bays and only 92 Nanosats. The fine Sun sensor and the horizon scanner are located in the DS in an unoccupied bay.

The mass and orbital average power of the ACS is given in the table below.

Table 15. Mass and Power of the ACS Subsystem

Component	Mass (Kg)	Power (Watts)
6 Coarse Sun Sensors	1.5	3
Fine Sun Sensor	1.4	N/A
Fine Sun Sensor Electronics	1	0.6
Earth Sensor	.2	.2
Laser Gyro	3	10
Total	7.1 kg	13.8 W

Command and Data Handling (C&DH) Subsystem

The requirements placed on the C&DH (avionics module) subsystem for the DS are as indicated in **Table** 16:

Table 16. C&DH Requirements

Item	Requirement
Power	2 Watts
Weight	12 kg
Operating Temperature	0 – 50 Degrees C
Radiation	40 kRad Si (Total Dose)
Data Rate From Telemetry	2 kbits/s
Data Storage	2 Gbits
Uplink/Downlink Protocol	CCSDS
Uplink Rate	1 kbits/s
Downlink Rate	100 kbits/s

The avionics module is based on a central processor. The subsystem also consists of a solid-state recorder to store data that will be transmitted to the ground stations for distribution to the end user. The Avionics module includes interfaces to the (ACS), the power subsystem, and the communications subsystems as well as the release actuators. The avionics module is responsible for sending commands, gathering telemetry data, processing the data, storing the data using Consultative Committee for Space Data Systems (CCSDS) packets, time tagging the data, and transmitting the stored data to the ground. The avionics module will be a processor-based system which will process commands, packetize the data, perform the timekeeping functions, perform ACS computations and control power. Data will be taken from the bus by the processor where the data will be manipulated into the required format. The avionics module will contain 2.0 Gbits of RAM. The avionics module will interface to the ACS subsystems Earth/Sun Sensor (analog data), Attitude Thruster (pulse command), Orbit Thruster (single pulse), the latch valves and the pyro actuated valves. The housekeeping functions include reading the thermistors, pressure transducers,

reading the voltage and current monitors, and gathering other analog telemetry. These functions will be handled using a 12 bit A/D converter. The Uplink/Downlink interface is connected directly to the transmitter and receiver. This interface sends CCSDS packet telemetry to the ground antennae, and receives CCSDS packet commands from the ground antennae and processes them.

A block diagram of the dispenser ship architecture is shown in *Figure* 24. The avionics module takes the form of a stack of Multi Chip Module (MCM) that will serve as the packaging technology for use by the Avionics module. For commonality with the Nanosat C&DH, the MCM module was selected for the DS. The stacked MCM will be composed of six functional interfaces, each of which will perform separate functions required by the avionics module. These functions are the processor, the memory, the actuator interface, the ACS interface, the housekeeping interface, and the communications interface. The development of these interfaces will require the extensive use of Field Programmable Gate Arrays (FPGAs). These FPGAs will be developed in a low power technology.

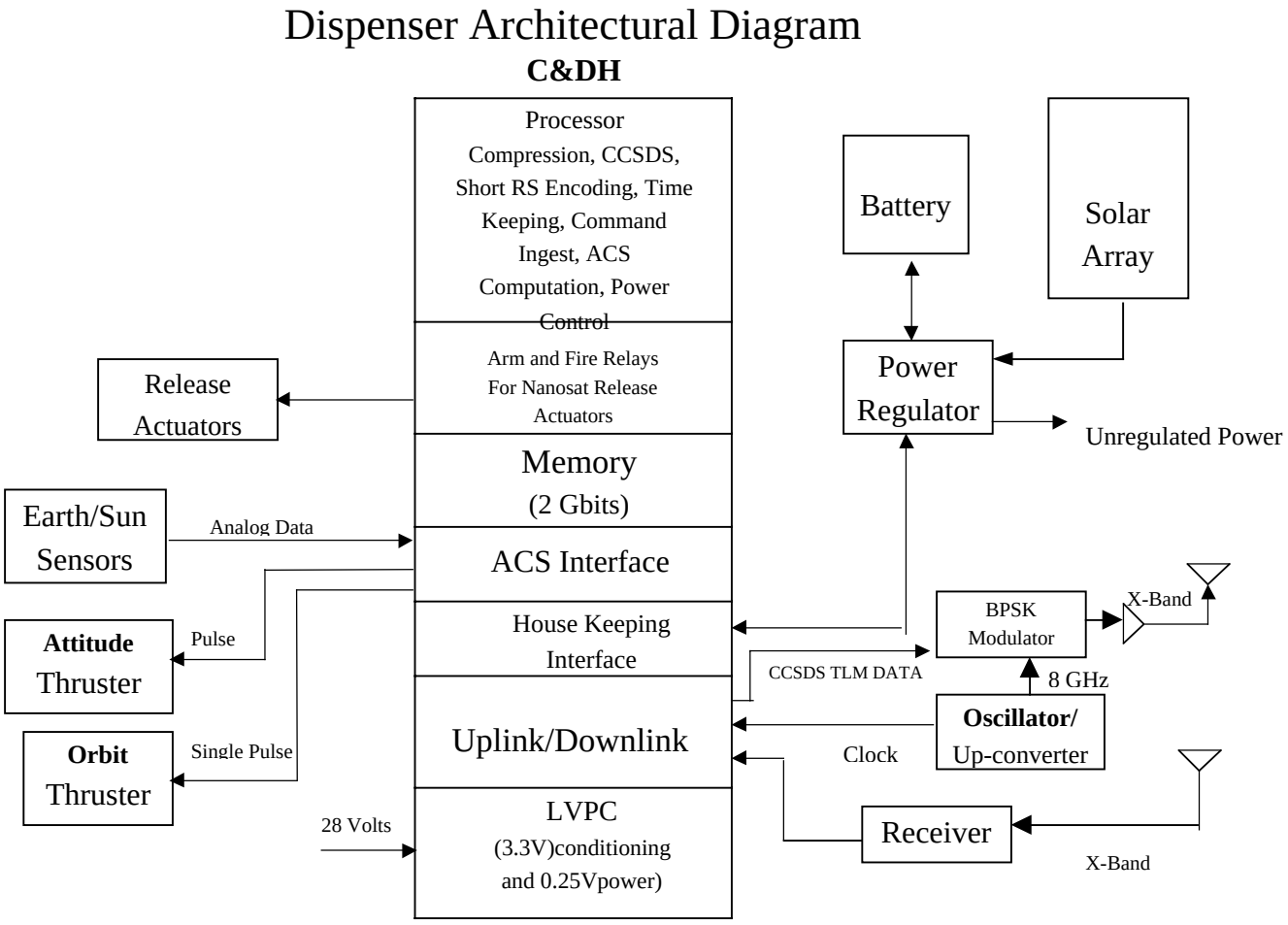

Figure 24. Dispenser ship architectural diagram.

Communications Subsystem

The communication system for the DS consists of a transmitter, receiver and an omni antenna. It operates in the X band. The up link/ down link frequencies are 7209.125 and 8470.XXX MHz (requested). The link analysis shows positive margin with an 11 meter ground station antenna and an omni antenna on the DS. The G/T ratio for the

ground segment must be 35.4 dB/°K in the X band. The EIRP from the DS is 1.76 db_w (1.5 watts in to antenna). To be compliant with the system requirement, using one-way Doppler for tracking, the oscillator must be stable to 5 x 10^{-8} per day. The down link transmission rate can be as high as 100 Kb/sec. and the command rate is baselined as 1 Kb/sec. (NB: downlink rates of up to 640 Kbps have been determined to be feasible, since this study).

Table 17. Mass and Power for the Communications System

Item	**Mass (Kg)**	**Power (Watts)**
Transmitter	2.27	3.2
Receiver	3.86	4
Oscillator/Diplexer	1.1	Negligible
Antennas	.6	N/A
Total	**7.83**	**7.2**
Allocated	12	11.2

Power Subsystem

The baseline requirements of the power subsystem are:

- The DS shall deliver no power to the Nanosats either while in orbit or on the ground (The requirement was imposed to eliminate the need for a connector between the Nanosat and the DS As a result he requirements on the flyaway mechanisms and ships wiring are eased)
- The subsystem will deliver at 28 V DC to the DS.
- 100 watts orbital average is required (although the spreadsheet shows approximately 78 watts are needed the 100 W requirement was imposed because it gave ample margin with little effect on the DS design)
- The launch of the DS will be timed to prevent eclipses longer than 40 minutes (this requirement decreased the battery capacity needed to operate thru the eclipse and eased the thermal design of the un-powered Nanosats)
- The DS lifetime shall be less than 3 months

Referring to *Figure* 25, the power subsystem consists of three main elements, the solar array which converts solar energy to electrical power, the regulators which, as the name implies, reduces the variation of the voltage on the power bus and the Lithium Hydride battery. The output to the bus will be 28±7v DC. The solar array is sized to deliver 130 watts off the array at BOL.

Table 18. Mass and Power of the Power Subsystem

Item	Mass Kg	Power Watts
Solar Array	3.6	N/A
Battery	1	N/A (recharge loss factored in by increasing the array size)
Regulators	1	32
Total as designed	5.6	32
Allocation	6.3	26

The power system was selected for its simplicity and reliability. By not supplying power to the Nanosats the need for breakaway connectors was eliminated, the amount wiring was reduced and the power requirements was also reduced. Operating at 28V is conventional which eliminates the interface problem with the Propulsion and ACS system components and permits the use of smaller gauge wire as compared to a 3 volt system.

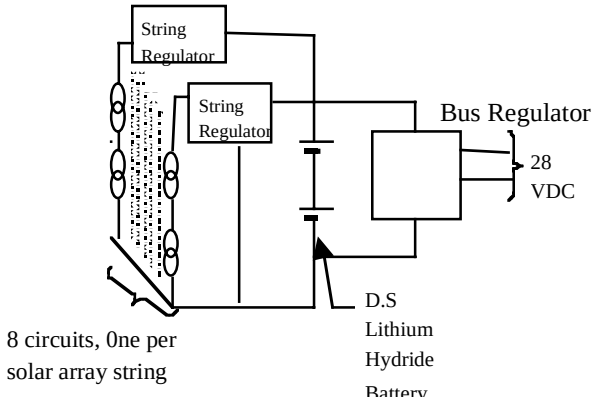

Figure 25. Power subsystem block diagram

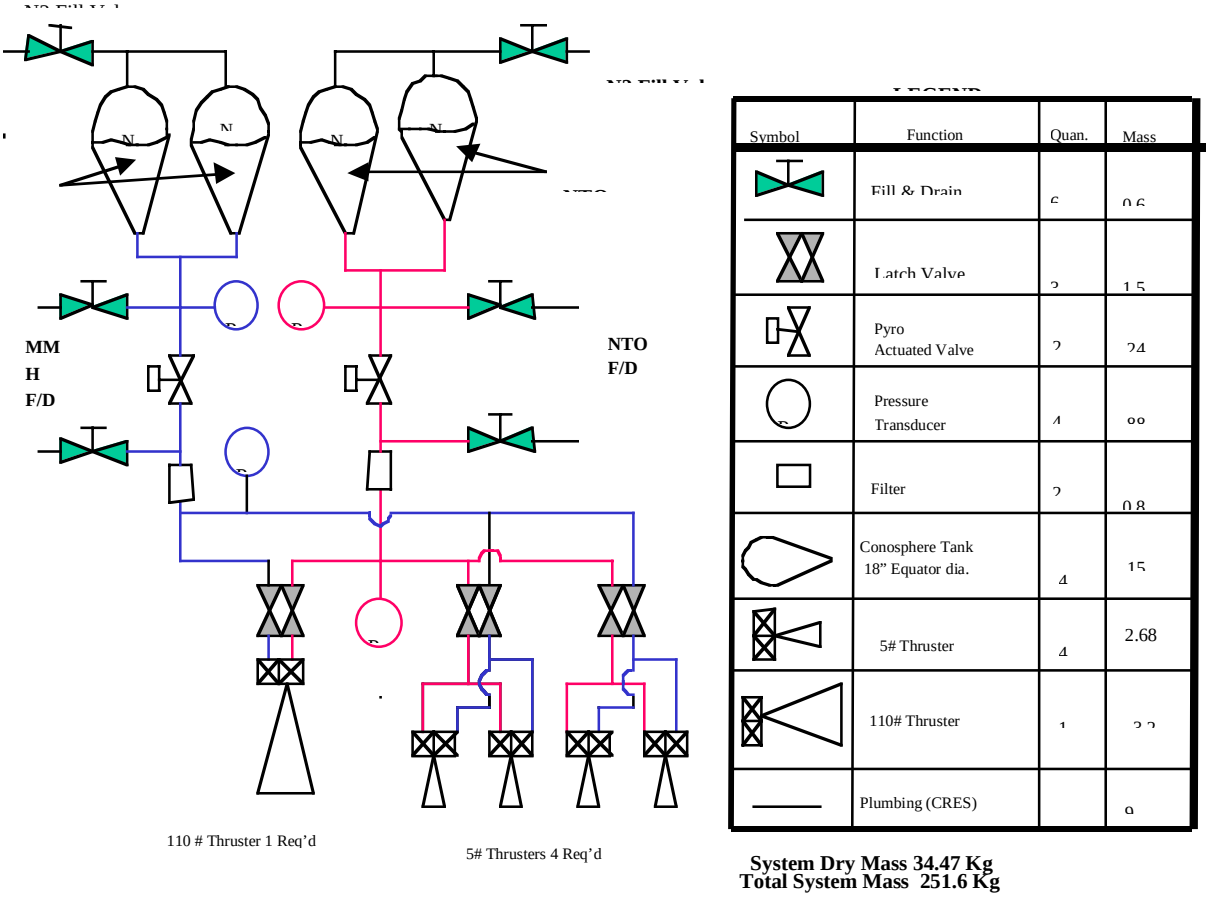

Figure 26. Propulsion System Block Diagram.

Propulsion Subsystem

Figure 26. is a diagram of the DS propulsion system. It is required to have 202 Kg of bi-propellant. The inert mass of the system shall not exceed 60 Kg. It must operate properly while the DS is spinning at 30rpm. The system will be used for adding delta-V, precessing the spin axis, controlling the spin rate and maintaining attitude control. The large thruster will be used for delta V maneuvers and the smaller thrusters will be used for the other functions. The pyro valves are opened after the DS has been placed in orbit by the launch vehicle. This action, arms the system. The thrusters will not fire until the latch valves are commanded open. The main engine latch valve will be kept closed and opened when a Delta V maneuver is immanent. The other latch valves will be left open and closed only if a thruster malfunctions. The estimated mass of the inert elements is shown in the inset of *Figure* 26. The total is 34.47 Kg, which is below the allotted 50 Kg and below the spreadsheet mass of 64.7Kg. The thrusters are fired infrequently and therefore the orbital average power is negligible.

Structure

The D.S structure consists of the inner structure and 7 berthing rings. The inverted cone at the base of internal support transition cylinder interfaces with the launch vehicle payload adapter fitting. Attached to this cylinder are 7 vertical gussets, which support the 7 Nanosat berthing rings. Detailed views of these structures are shown in the full report from which this information is taken. *Figure* 27 shows an external view of the dispenser ship showing the major dimensions.

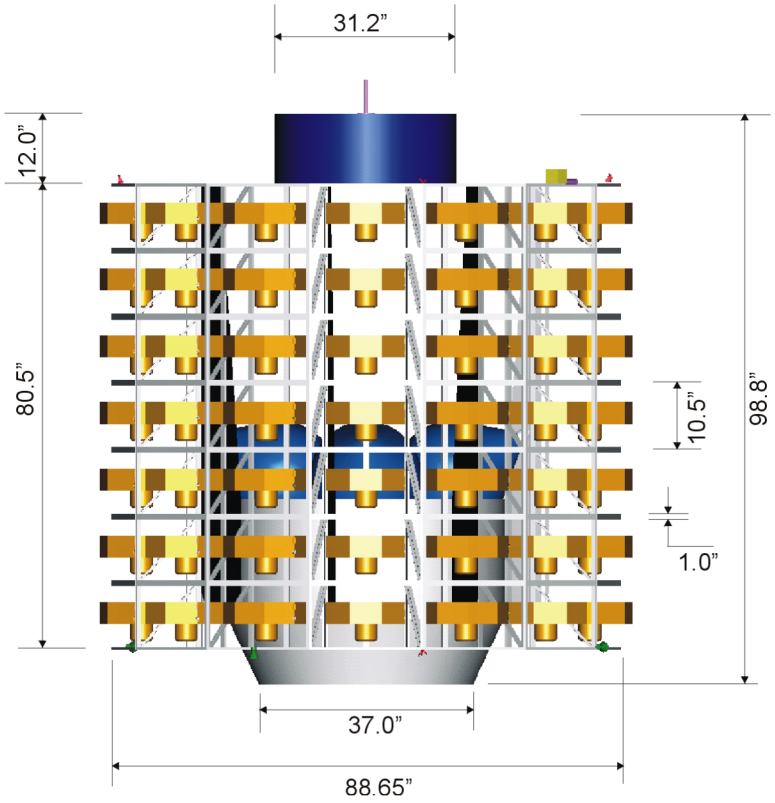

Figure 27. Dispenser Ship overall structure and dimensions.

Inner Structure

The propulsion system's four tanks and the large thruster are carried by the inner structure. The four small thrusters are located on the lower berthing ring. Two of the thrusters are for spin control, a third is used for precession control and the fourth is a backup for the precession control thruster. In addition, the inner structure carries the three coarse sun sensors. Additional detail and figures are shown in the full dispenser ship report.

Table 19 lists the mass properties of the dispenser ship structural components. The moment of inertia has been calculated for the beginning as well as the end of life (detailed numbers are contained in the full dispenser ship report). As stated before, the data indicates the D.S. will be stable as a spinner.

Table 19. Mass of the Structural Subsystem

Elements	Mass/Weight (lbs)	
	lbs	Kg
Support Gussets	35	16
PAF	31.2	14
Propulsion Deck	11.7	5.3
Ring Assy. Upper (4 decks)	82	37
Ring Assy. Lower (3 decks)	129	59
Total	288.9	131.3

Thermal Subsystem

Similar to the Nanosat spacecraft, preliminary study results indicate that the Nanosat DS thermal requirements can be accommodated with a passive thermal control system (blankets, heaters, and coatings). The MLI will be used on top and bottom to reduce losses and gains from the environment. The cylindrical sides (shell) of the DS are not insulated. Heaters and MLI may be used to maintain propulsion lines and thrusters during orbit changes.

The thermal analysis used 0.3 for the Albedo factor, a solar constant of 1351.43 W/sq.m and a planet power of 237.805 W/sq.m. **Table** 20 lists the parameters and thermal characteristics that were used in the thermal analysis:

Table 20. Thermal Design Parameters

Parameter and Characteristics	Comments
Orbit	Perigee = 3 $R_{e,}$ Apogee = 20 $R_{e,}$ Inclination Angle = 7.5° Period = 2.43 Days, No eclipse
Mission Life time	2 months
ACS	Spin stabilized, spin rate of at least 20 rpm and spin axis aligned to ±5° of ecliptic pole. Short excursions TBD from this design attitude can be tolerated.
Temperatures	DS operating temperature range of 0° to +50°C Nanosat temperature requirement of –20 to +50°C for survival, non-operating mode,
Thermal Configuration	Nanosats are mounted around the drum of the DS, but isolated from birdcage and DS shell Nanosats are not powered up while on the DS components are mounted internally on decks, which are in turn conductively coupled to the DS shell. The shell is radiatively and conductively coupled to the top and bottom decks Berthing Ring is conductively coupled to the DS shell The nozzle is coupled to the bottom deck.
Solar Array	The DS solar array is coupled to the top deck. Operating temperature -100 to +40°C (+80°C survival upper limit)
Power Dissipation	The DS dissipates a total of 100 watts, orbit average, assumed distributed evenly on the DS shell

A top -level thermal analysis has been completed. For the most part, each component of the dispenser was modeled as a single node and the individual spacecraft were modeled as five nodes each. For components that are mounted externally, have a high watt density, or have tight temperature control requirements, a more detailed model would need to be completed.

Preliminary results indicate that the Nanosats mounted in the top ring run slightly warmer than the others, while the ones in the bottom ring run the coolest. The DS temperature is set by the high energy absorbed by the shell and it's conductive coupling to the birdcage. Since the surfaces of the Berthing Ring were painted white, they ran colder than any of the other surfaces. When the dispenser ship was conductively coupled to the Berthing Ring its temperatures were on the order of 10°C colder than when it was isolated from the Berthing Ring. Therefore, the coupling between the shell and Berthing Ring is important and should be examined more closely in future studies. Nonetheless, the simple design described above, is reliable and appears to meet temperature requirements for the DS as well as the Nanosats. Further parametric analysis should be conducted with a more detailed model.

3.3.4. Launch Vehicle

The launch vehicle assumed for the Magnetotail Constellation mission is the Delta II 7925 vehicle with a 9.5 ft fairing. This vehicle is a 3-stage vehicle. The 1st stage has a liquid engine with nine attached solid propellant graphite epoxy motors. The 2nd stage also has a liquid rocket engine. The 3rd stage carries the DRACO Payload (DS and the complement of Nanosats) which is attached to the 3rd stage via a clamp band separation system. The launch vehicle will separate the Dispenser ship placing it and it's Nanosats into a 1.15 x 20 R_E orbit.

3.4. Integration and Test

Of particular importance to the DRACO Mission will be innovation in the way in which the payloads (Nanosats) are integrated to the dispenser ship. The normal way of integrating payloads to the main spacecraft would result in an unacceptably long and costly integration period. This section discusses ways of approaching this issue. It will be assumed that each Nanosat bus and instrument suite will be delivered as a single, ready-to-integrate system. That is, rather than treating the Nanosat bus as separate from the Nanosat instrument suite, they will be treated as a single entity, or “sciencecraft”, when integrated to the DS. Furthermore, each Nanosat must not take longer than 1 or 2 days to fully integrated to the DS. One can see this is necessary, as the integration of 92 Nanosats taking 2 days each would be 184 days, or 6 months of 7 day per week operation if the Nanosats are integrated in a serial fashion. If a few or several Nanosats can be integrated in parallel, this would reduce the integration time, but could increase integration cost due to higher manpower requirements.

One approach to mitigating this issue is to design the Nanosat for rapid integration thru the use of highly automated processes and test equipment. This would require development of automated test equipment and processes, or, requires that the design process take into account the use of existing test equipment and processes to optimize the ability to quickly test the “sciencecraft”.

Another approach is to accept more risk in the process by only completely testing every nth unit and performing reduced testing on the other units. This approach means that more risk must be accepted. This type of testing is frequently done by the Department of Defense and various commercial companies on large lots of identical systems (e.g., missiles, Iridium spacecraft). These processes should be studied to find out any “lessons learned” and to help understand if this type of testing would be an acceptable risk for the Magnetostail Constellation DRACO Mission. Again, thought should be given to the likelihood of this type of testing during the design process. It is possible that the risk inherent in this type of test approach can be reduced by careful and clever design.

3.5. Mission Operations

The operation of a constellation of identical Nanosatellites requires different concepts than for single spacecraft missions. The Nanosatellites may be constrained in the amount of functions they can perform onboard by the lack of processing power. The large number of spacecraft requires automation on the ground in order to keep the staffing to a reasonable level and offers an opportunity for changes in risk management. The loss of a few spacecraft over the mission lifetime is tolerable for this mission.

Routine operations commence after the Nanosatellites have reached their operational orbit. Routine operations are only interrupted by anomalies or infrequent events such as eclipse.

3.5.1. Space/Ground communications

There are several options for space/ground communications services - dedicated stations, commercial networks, NASA stations, large antennas, smaller antennas, etc. This operations concept assumes the use of a commercial network of 11-meter antennas. The commercial network would have a number of these antennas distributed around the world. Communications would only occur around perigee. At some points in the mission, as many as two-dozen spacecraft might be near perigee at the same time. The multiple stations would be able to handle some of these

spacecraft. Spacecraft with smaller apogees could skip a contact, and dump their data at the next perigee. Loss of some data during these infrequent “traffic jams” would be acceptable - the overall data completeness requirement will be ~95%.

The ground stations will provide telemetry, commanding, and tracking services. The real-time housekeeping data will be extracted from the downlink data and sent to the operations center in real-time. Playback science and housekeeping data and tracking data will be sent to the operations center after the contact, sharing the bandwidth with other station users.

3.5.2. Planning and Scheduling

The scheduling of the ground stations depends on how the ground station services are provided. One option would be to let the ground station provider schedule the contacts within provided guidelines for data completeness and frequency of tracking data collection. The ground station provider would have the flexibility to adjust the contacts within these guidelines, which potentially could result in lower costs to the project. The ground station provider would provide the schedule to the operations team so then they could identify uplink opportunities and support data accounting.

3.5.3. Commanding

The spacecraft will be commanded every contact to initiate the downlink of data. Since the ground station schedule is subject to change, particularly for the spacecraft with distant apogees, the downlink cannot be initiated by the spacecraft. The instrument scripts may be updated once every month or so. The instrument script may be as simple as timed tagged commands or could be a more sophisticated set of instructions for the onboard system to interpret. Software loads may be performed if problems are identified after launch that can be addressed by the flight software. The data system will automatically uplink new loads or instrument scripts to the constellation. The loads will have a time window within which each spacecraft must be updated. The system will automatically send and verify the load during regularly scheduled contacts. The operators will be alerted of any spacecraft that is not updated when the window closes.

3.5.4. Housekeeping Data Processing

The data system will automatically process the housekeeping data and identify limits violations and improper configurations. The system will be capable of processing data from multiple spacecraft simultaneously. The data system will also process status information from the ground station and identify any missing or poor quality data. Problems will be ranked according to severity. Significant problems will result in an immediate alert to the operations team. If the operations team is not present, the system will use a pager to notify them. The data system will process all of the housekeeping data and produce standard analysis reports. These reports will compare telemetry parameters across time and across spacecraft. Spacecraft engineers will be able to generate custom reports as well.

3.5.5. Science Data Processing

The science data is automatically level-zero processed when it is received from the ground station. This processing removes overlaps in the data and identified missing data. Operators are alerted in the event that a significant amount

of data is missing. The system will have data accounting tools to assist the operators in visualizing the data loss and its distribution over the constellation. The operators will work with the ground station network to attempt to recover lost data that exceeds requirements. They may adjust the scheduling priorities if some part of the constellation is losing more data than other parts. The data will be automatically processed into standard products and archived in the science center. It will be distributed to science users electronically or, for large amounts of data, on physical media.

3.5.6. Operations Staffing

The mission operations staff (not including the science operations staff) for the Magnetotail Constellation DRACO can be relatively small. The spacecraft are performing survey missions and have limited reconfiguration capability. The ground systems are automated, performing all routine functions. The operations team will primarily handle exceptions that have been flagged by the data system. The operations teams primary concern will be for common problems that have the potential to affect all of the members of the constellation. The nominal oeprations staff will be about six people. It will include one or two spacecraft engineers, a science liason member, a data accounting person, and an orbit expert. The operations staff will work 40 hours per week, and at least one member will be on call for automated alerts during off-hours.

3.5.7. Special Operations

At launch, the operations team will be augmented with personnel from the spacecraft development and test functions. The ground data system may include more ground stations or larger ground stations, to checkout and track the spacecraft after deployment. The ground system will also have to operate the DS during this phase of the mission. The deployment operations may be adjusted (e.g., to change the number of spacecraft deployed at a time, or change the frequency of deployment), based on the experience with the first few deployments.

In the event of an anomaly, the operations team may request the assistance of the spacecraft developers to identify the cause of a problem and to develop corrective action or work arounds. The spacecraft developer will be responsible for maintaining the flight software throughout the mission. To assist in the anomaly resolution, the operatins team may use larger ground antennas to communicate with the spacecraft over longer periods of time, rather than just at perigee.

3.6. Schedule

Table 21. **Magnetotail Constellation Development Schedule**

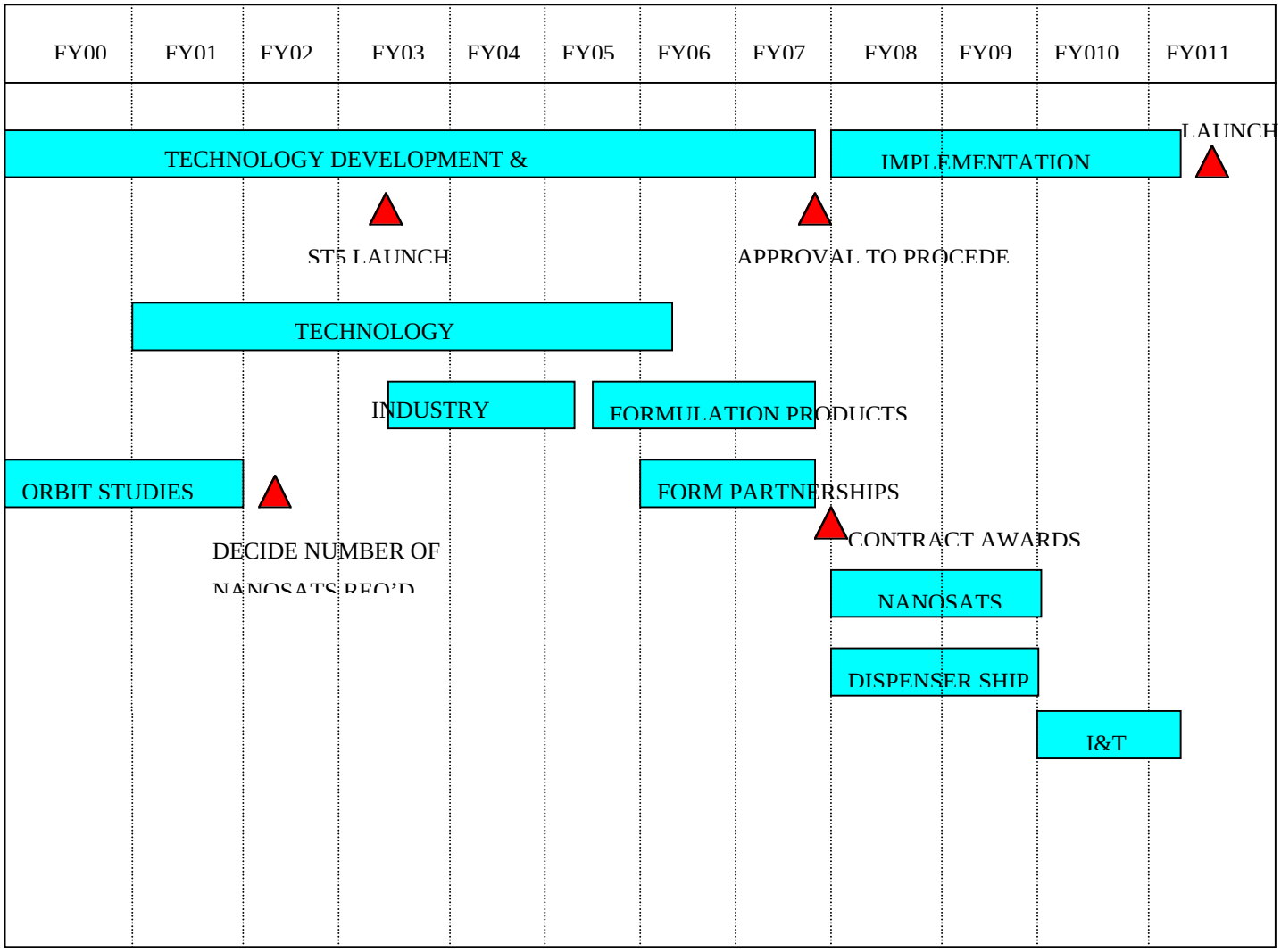

4. Mission Enabling Technology Development

To realize the Magnetospheric Constellations Mission, a number of enabling technologies must be developed and matured. These technologies are listed below:

- Miniaturized, low power, radiation hardened analog and digital electronics
- Advanced propulsion systems
- Avionics on a chip
- Lightweight, high capacity batteries
- Lightweight, low power communications components
- Software tools for autonomous ground operations of satellite constellations
- Data acquisition, distribution and visualization from constellations

In addition to these technologies, new tools and methodologies must be developed for manufacturing large numbers of research grade instruments and satellites at low cost, and testing and integrating these large numbers of nanosatellites in a reasonable amount of time. These particular issues will be discussed in greater detail in the sections to follow.

4.1. Instrumentation

Development of instrument technologies and instruments of mass and power commensurate with a Nanosatellite class mission are well underway by DOD, NASA and various other institutions and agencies, both U.S. and international. Some instruments, such as magnetometers, are already close to the mass and power needed for a constellation mission. The issues of most significance in the development of instruments for a constellation mission are recurring cost and capability to be manufactured in large quantities in a reasonable period of time. The current paradigm of a 2-3 year instrument development, fabrication and qualification period with costs typically in the several hundred thousand to over one million dollar cost range is clearly unacceptable when one wishes to fabricate and qualify as many as 100 identical sets of instruments. It is this “manufacturability” issue that most needs to be addressed by the Magnetotail Constellation DRACO Mission, especially in light of the possibility that some instrument technologies may require new designs to achieve the cost and “manufacturability” requirements.

The strategy to be pursued by the Magnetotail Constellation Mission includes the following options:

- NASA Research Announcements (NRAs) initiated and funded through DRACO formulation efforts
- Leveraging of NASA HQ initiated and funded NRAs (directed DRACO funding to supplement these efforts)
- Participation in, or leveraging of, other proposal opportunities such as the Cross Enterprise Program.
- Spinoff from the ST-5, Nanosatellite Constellation Trailblazer project under the New Millenium Program.

Another approach under consideration involves the partnering of scientists and instrument developers with the developers and builders of spacecraft buses to create an integrated “sciencecraft”. This approach will be discussed in a little more detail in the next section.

4.2. Nanosatellite Development

In contrast to instruments, a number of technologies (as listed above) need to be developed and matured before a Nanosatellite meeting the DRACO requirements can be realized. As with the instrument technologies, a number of agencies and institutions, both domestic and international are actively working on Nanosat technologies. In many cases, these technologies are being funded at the subsystem level of development (eg, avionics on a chip or miniaturized propulsion systems), with emphasis placed on the technology of most interest by the organization providing the money. The DRACO Mission will track these activities and wherever possible leverage these development efforts. One potential near term opportunity is to work closely with the recently awarded ST-5 mission, Nanosat Constellation Trailblazer. Efforts are already underway to establish a relationship with the ST-5 project office at Goddard Space Flight Center.

The same issues of non-recurring cost and "manufacturability" apply to the spacecraft. In addition, however, there is the issue of integration and testing at the laboratory level (instruments and spacecraft). Although some efforts at development have begun in these areas (e.g., NRO Directors Innovation Initiative NRO000-99-R-0176), the issue as it applies to DRACO must be addressed. Although the spacecraft "manufacturability" issues can be addressed through the use of NRA's and RFP's, a more integrated approach has been suggested for the DRACO mission.

It is thought that all of the manufacturability issues might be addressed by teaming a science group with a spacecraft vendor. In this fashion, an integrated approach can be taken from the very beginning, at the design level. Innovative methods of testing must be developed to greatly reduce the time required; this can be accomplished through hardware design, software development or a combination of both. Test methods and hardware can be designed concurrently with the instrument and spacecraft development process. Instrument and spacecraft designs would be influenced by how easily and quickly integration could be done. At the present time, it is not clear what mechanism would be used to create or encourage the partnership of the science teams and the spacecraft teams.

4.3. Constellation Operations Management and Autonomy

In order to manage a large constellation of Nanosatellites during the operations phase at a reasonable cost, a significant degree of autonomy on the ground as well as on-board the nanosats will be required. There is already an existing base of experience and knowledge, along with the hardware and software tools, that resides in the commercial world – in particular, the Iridium communications constellation. It is expected that the DRACO formulation efforts will learn and build upon this knowledge base, developing new tools and methods as required for a scientific constellation. To the extent that the commercial world is aware of the push for future science missions that consist of large constellations of spacecraft, there is already some evolution of the ground operations tools and methodologies to accommodate this.

In the area of spacecraft autonomy, there is already a significant amount of interest in this area, with work being funded thru numerous channels. The DRACO mission will require as a minimum the capability for on-board error detection and correction and the ability to operate for days or weeks at a time without ground intervention, but to a large extent these capabilities already exist. A greater degree of sophistication will be required for the DRACO Mission and it is possible that new requirements will be levied in this area as the formulation effort progresses. At the current time, however, the exact degree of autonomy and detailed requirements for the DRACO Mission have not been determined beyond the basic requirements mentioned above.

4.4. Advanced Data Assimilation and Handling Techniques

It is widely recognized that the data sets generated by constellation missions require data management and handling techniques that are outside the current experience with space missions. Nevertheless, the problem is not qualitatively different from that associated with the conduct of atmospheric meteorology research and monitoring.

The most fundamental problem is the visualization of both scalar and vector field information from a large number of observing stations. Some techniques developed for meteorology will be directly transferable to use with constellation data sets. Others will require new techniques, for example the visualization of magnetic field information that is not present in atmospheric meteorology.

The next step beyond basic visualization is the assimilation of the data into global circulation models. This will allow for instantaneous comparison with such models, extrapolation of the observations into other parts of the system outside the constellation, and projection or forecasting of system behavior for comparison with actual observed system evolution. This is a complex process, which has been discussed in much more detail in the section on science objectives, above.

Because the treatment of constellation data is so foreign to space physics, there is a significant need for the development of appropriate tools, borrowing wherever possible from prior work along the same lines that has already been completed in meteorology. As an integral part of the technology development effort for DRACO, developments along these lines should be supported at appropriate institutions with expertise in visualization and assimilation of data. Researchers who are active in the global simulation of magnetotail processes should undertake a significant amount of this work. They are in a position to generate simulated data sets, to introduce realistic errors in them, and then to develop the means to reassimilate the simulated data back into the same model that generated it, or other independent models.

5. Selected References

Akasofu, S.-I., The development of the auroral substorm, Planet. Space Sci., 12, p.273, 1964.

Angelopoulos, V., C. F. Kennel, F. V. Coroniti, R. Pellat, H. E. Spence, M. G. Kivelson, R. J. Walker, W. Baumjohann, W. C. Feldman, J. T. Gosling, and C. T. Russell, Characteristics of ion flow in the quiet state of the inner plasma sheet, Geophys. Res. Lett., 20, 1711, 1993.

Angelopoulos, V., C. F. Kennell, F. V. Coroniti, R. Pellat, M. G. Kivelson, R. J. Walker, C. T. Russell, W. Baumjohann, W. C. Feldman, and J. T. Gosling, Statistical characteristics of bursty bulk flow events, J. Geophys. Res., 99, 21257, 1994.

Baker, D.N., R. C. Anderson, R. D. Zwickl, and J. A. Slavin, Average plasma and magnetic field variations in the distant magnetotail associated with near-Earth substorm effects, J. Geophys. Res., 92, 71, 1987.

Baker, D.N., T.I. Pulkkinen, V. Angelopoulos, W. Baumjohann, and R.L. Neutral line model of substorms: Past results and present view, J. Geophys. Res., 101, 12,975, 1996

Baumjohann, W., G. Paschmann, and H. Luhr, Characteristics of high-speed ion flows in the plasma sheet, J. Geophys. Res., 95, 3801, 1990.

Birn, J., M. Hesse, and K. Schindler, MHD simulations of magnetotail dynamics, J. Geophys. Res., 101(A6), p.12939, 1996.

Borovsky, J. E., R. C. Elphic, H. O. Funsten, and M. F. Thomsen, The Earth's plasma sheet as a laboratory for flow turbulence in high-beta MHD, J. Plasma Phys., 57, 1, 1997.

Calder, Nigel, The Weather Machine, Penguin Books, Middlesex, UK, 1977.

Dungey, J., Inaugural Lecture as Professor of Physics at Imperial College, 1966; quote courtesy of W. J. Hughes.

Fairfield et al., Geotail observations of substorm onset in the inner magnetotail, J. Geophys. Res., 103, 103, 1998.

Ghil, M., K. Ide, A. F. Bennett, P. Courtier, M. Kimoto and N. Sato (Eds.), 1997: Data Assimilation in Meteorology and Oceanography: Theory and Practice, Meteorological Society of Japan and Universal Academy Press, Tokyo, 496 pp.

Hayakawa, H., A. Nishida, E. W. Hones, and S. J. Bame, Statistical characteristics of plasma flow in the magnetotail, J. Geophys. Res., 87, 277, 1982.

Henderson, M. G., G. D. Reeves, H. E. Spence, R. B. Sheldon, A. M. Jorgensen, J. B. Blake, and J. F. Fennell, First energetic neutral atom images from POLAR, Geophys. Res. Lett., 24, 1167, 1997.

Hoshino, M., T. Mukai, A. Nishida, Y. Saito, T. Yamamoto and S. Kokubun, Evidence of two active reconnection sites in the distant magnetotail, J. Geomag. Geoelectr., 48, 515, 1996.

Jacquey, C., J.A. Sauvaud, and J. Dandouras, Tailward propagating cross-tail current disruption and dynamics of the near-Earth tail: a multi-point measurement analysis, Geophys. Res. Lett. 20(10), 983, 1993.

Jorgensen, A. M., H. E. Spence, M. G. Henderson, G. D. Reeves, M. Sugiura, and T. Kamei, Global energetic neutral atom (ENA) measurements and their association with the Dst index, Geophys. Res. Lett., 24, 3173, 1997.

Li, X., D.N.Baker, M.Temerin, G.D.Reeves, and R.D.Belian, Simulation of dispersionless injections and drift echoes of energetic electrons associated with substorms, Geophys. Res. Lett., 25(20, p.3763, 1998.

Lieberman, A., NASA-GSFC Magnetospheric Constellation Mission Document, NASA GSFC Code 730, 30 March 1999a.

Lieberman, A., Final Report: Nonosat Dispenser Ship Performance Feasibility Study for the Magnetospheric Constellation Mission, NASA GSFC Code 730, Swales Aerospace report SAI-RPT-284, 22 July, 1999b.

Lopez, R.E., H.E.J. Koskinen, T.I. Pulkkinen, T. Bösinger, R.W. McEntire, and T.A. Potemra, Simultaneous observation of the poleward expansion of substorm electrojet activity and the tailward expansion of current sheet disruption in the near-Earth magnetotail, J. Geophys. Res. 98(A6), 9285, 1993.

Lui, A.T.Y., C.-L. Chang, A. Manofsky, H.-K. Wong, and D. Winske, A cross-field current instability for substorm expansions, J. Geophys. Res., 96, 11389, 1991.

Lui, A.T.Y., Current disruption in the Earth's magnetosphere: Observations and models, J. Geophys. Res., 101(A6), p.13067, 1996.

McIlwain, C. E., Comments and Speculations concerning the Radiation Belts, *in* Proceedings of the Joint IQSY/COSPAR Symposium, London, 1967, Part 1, MIT Press, Cambridge, MA, USA, p.303, 1967.

McPherron, R. L., C. T. Russell, and M. P. Aubrey, Satellite studies of magnetospheric substorms on August 15, 1968, 9, Phenomenological model for substorms, J. Geophys. Res., 78, p.3131, 1973.

Miller, R. N., M. Ghil, and F. Gauthiez, Advanced data assimilation in strongly nonlinear dynamical systems, J. Atmos. Sci., 51, 1037, 1994.

Moore, T. E., R. L. Arnoldy, J. Feynman, and D. A. Hardy, Propagating Substorm Injection Fronts, J. Geophys. Res. 86, 6713, 1981.

Mukai, T., M. Fujimoto, M. Hoshino, S. Kokubun, S. Machida, K. Maezawa, A. Nishida, Y. Saito, T. Teresawa, and T. Yamamoto, Structure and kinetic properties of plasmoids and their boundary regions, *J. Geomag. Geolectr., 48*, 541, 1996.

Nagai, T., M. Fujimoto, Y. Saito, S. Machida, T. Teresawa, R. Nakamura, T. Yamamoto, T. Mukai, A. Nishida, and S. Kokubun, Structure and Dynamics of magnetic Reconnection for Substorm Onsets with GEOTAIL observations, *J. Geophys. Res., 103,* 4,419, 1998.

Ohtani, S.-I., Earthward expansion of tail current disruption: Dual-satellite study, J. Geophys. Res., 103(A4), p. 6815, 1998.

Raeder, J., J. Berchem, M. Ashour-Abdalla, L. A. Frank, W. R. Paterson, K. L. Ackerson, R. P. Lepping, S. Kokubun, T. Yamamoto, and S. A. Slavin, Boundary layer formation in the magnetotail: Geotail observations and comparisons with a global MHD model GRL, 24, 951, 1997.

Reeves, G. D., R. W. H. Friedel, M. G. Henderson, A. Korth, P. S. McLachlan, and R. D. Belian, Radial propagation of substorm injections, International Conference on Substorms-3, ESA SP-339, 579-584, 1996.

Schindler, K., A theory of the substorm mechanism, *J. Geophys. Res., 79*, 2,803, 1974.

Slavin, J.A., D.H. Fairfield, M.M. Kuznetsova, C.J. Owen, R.P. Lepping, S Taguchi, T. Mukai, Y. Saito, T. Yamamoto, S. Kokubun, A.T.Y. Lui, and G.D. Reeves, ISTP Observations of Plasmoid Ejection: IMP 8 and Geotail, *J. Geophys. Res., 103,* 119, 1998.

Slavin, J.A., M. F. Smith, E. L. Mazur, D. N. Baker, T. Iyemori, and E. W. Greenstadt, ISEE 3 observations of traveling compression regions in the Earth's magnetotail, *J. Geophys. Res., 98,* 15,425, 1993.

Song, Y., and R. L. Lysak, Turbulent generation of auroral currents and fields -- A spectral simulation of two-dimensional MHD turbulence, in Modeling Magnetospheric Plasma, T. E. Moore and J. H. Waite (eds.), pp. 197, AGU, Washington, D. C., 1988.

Swift, D. W., Numerical simulation of the generation of electrostatic turbulence in the magnetotail, Geophys. Res., 86, 2273, 1981.

T. Tajima, Astrophysical Plasmas, Frontiers in Physics series, Addison Wesley, 1997.

Talagrand, O., Assimilation of observations, an introduction, J. Meteo. Soc. Japan, 75, 191, 1997.

Tsyganenko, N. A., and M. Peredo, Analytical models of the magnetic field of disk-shaped current sheets, J. Geophys.Res., 99, 199, 1994.

Tsyganenko, N. A., Modeling of twisted/warped magnetospheric configurations using the general deformation method, J. Geophys.Res., 103, 23551, 1998.